Multi-decadal mass balance series of three Kyrgyz glaciers inferred from modelling constrained with repeated snowline observations

Martina Barandun[1], Matthias Huss[1,2], Ryskul Usubaliev[3], Erlan Azisov[3], Etienne Berthier[4], Andreas Kääb[5], Tobias Bolch[6], and Martin Hoelzle[1]

[1]Department of Geosciences, University of Fribourg, Fribourg, Switzerland
[2]Laboratory of Hydraulics, Hydrology and Glaciology (VAW), ETH Zurich, Zurich, Switzerland
[3]Central Asian Institute of Applied Geosciences (CAIAG), Bishkek, Kyrgyzstan
[4]CNRS, LEGOS, University of Toulouse, Toulouse, France
[5]Department of Geoscience, University of Oslo, Norway
[6]Department of Geography, University of Zurich, Switzerland

Correspondence to: Martina Barandun (martina.barandun@unifr.ch)

Abstract.

Glacier surface mass balance observations in the Tien Shan and Pamir are relatively sparse and often discontinuous. Nevertheless, glaciers are one of the most important components of the high-mountain cryosphere in the region as they strongly influence water availability in the arid, continental and intensely populated downstream areas. This study provides reliable and continuous surface mass balance series for selected glaciers located in the Tien Shan and Pamir-Alay. By cross-validating the results of three independent methods, we reconstructed the mass balance of the three benchmark glaciers, Abramov, Golubin and Glacier No. 354 for the past two decades. By applying different approaches, it was possible to compensate for the limitations and shortcomings of each individual method. This study proposes the use of transient snowline observations throughout the melting season obtained from satellite optical imagery and terrestrial automatic cameras. By combining modelling with remotely acquired information on summer snow depletion, it was possible to infer glacier mass changes for unmeasured years. The model is initialized with daily temperature and precipitation data collected at automatic weather stations in the vicinity of the glacier or with adjusted data from climate Reanalysis products. Multi-annual mass changes based on high-resolution digital elevation models and in situ glaciological surveys were used to validate the results for the investigated glaciers. Substantial surface mass loss was confirmed for the three studied glaciers by all three methods, ranging from -0.30 ± 0.19 m w.e. yr^{-1} to -0.41 ± 0.33 m w.e. yr^{-1} over the 2004-2016 period. Our results indicate that integration of snowline observations into mass balance modelling significantly narrows the uncertainty ranges of the estimates. Hence, this highlights the potential of the methodology for application to unmonitored glaciers at larger scales for which no direct measurements are available.

1 Introduction

Glaciers are important components of the hydrological cycle in Central Asia. In this arid continental region, the intensely populated and irrigated downstream areas strongly depend on a supply of water from the cryosphere such as glaciers and snow (Kaser et al., 2010; Schaner et al., 2012; Duethmann et al., 2014; Chen et al., 2016; Huss and Hock, 2018). The uncertainty of

water availability in the context of a changing climate creates a major potential for political tension and builds a complex set of future threats, affecting different sectors such as water management, energy production and irrigation (Varis, 2014; Munia et al., 2016). Climate change poses a manifold challenge for the Central Asian population and will influence natural hazards and threaten future economies and the livelihood of coming generations (Stocker et al., 2013). For this reason, continuous and high-quality data for the different components of the hydrological cycle acquired within established regional and national cryospheric and hydrologic climate services are key for providing accurate predictions which enable sustainable adaptation. As stated by the World Meteorological Organization (GCOS, 2016), large gaps currently exist in the global climate observation system. This refers in equal measure to such remote and unmonitored areas especially in the Pamir, but also in the Tien Shan, where there is a lack of data crucially needed to plan and enhance future development (Sorg et al., 2012; Unger-Shayesteh et al., 2013). Improved temporal and spatial representation of glacier monitoring is thus essential, due to the paramount significance of glaciers in the high-mountain cryosphere.

During the Soviet era, in the 1950s and 1960s, an extensive system of cryospheric monitoring was launched in the Tien Shan and Pamir-Alay. Most programmes stopped abruptly after the breakdown of the USSR in the mid-1990s. Monitoring activities were maintained only on Tuyuksu Glacier, Kazakhstan, and Urumqi Glacier (No. 1), China. In recent years, different initiatives have aimed at the re-establishment of glacier monitoring in Central Asia (Hoelzle et al., 2017). Surface mass balance (SMB) series are now available for the following glaciers: Abramov (Pamir-Alay), Batysh Sook, Sary-Tor, Karabatkak and Glacier No. 354 (Central Tien Shan), for Urumqi No. 1 (Eastern Tien Shan) and for Golubin and Tuyuksu (Northern Tien Shan) (Fig. 1) (WGMS, 2013). However, a significant gap in the data from the mid-1990s to around 2010 hinder the interpretation of long-term trends in glacier behaviour in this region.

Different studies derived continuous mass balance series for selected glaciers based on modelling (e.g., Fujita et al., 2011; Barandun et al., 2015; Kronenberg et al., 2016; Liu and Liu, 2016; Kenzhebaev et al., 2017) and estimated mass balance at a regional scale in the Pamir-Alay and Tien Shan (Farinotti et al., 2015). Modelled mass balance series have a good temporal resolution; however, they are not observation-based and thus strongly depend on model calibration and the quality of the input variables. Several studies use remote sensing techniques to fill the gaps in glacier monitoring and to generate insights into region-wide mass changes covering entire High Mountain Asia within the past two decades (e.g. Gardner et al., 2013; Gardelle et al., 2013; Kääb et al., 2015; Brun et al., 2017; Wang et al., 2017). Furthermore, other authors focused on selected regions of the Central and Northern Tien Shan (e.g., Aizen et al., 2007; Pieczonka et al., 2013; Bolch, 2015; Pieczonka and Bolch, 2015; Goerlich et al., 2017) deriving glacier-specific geodetic mass balances. These studies often cover large areas, but temporal resolution is typically limited to five years or longer periods. Thus, they fail to capture the interannual or even seasonal signals.

The snowline is recognized as a valuable proxy for glacier mass balance (LaChapelle, 1962; Lliboutry, 1965; Braithwaite, 1984; Kulkarni, 2012; Rabatel et al., 2017). Different methods have been developed to use the end-of-summer snowline observed on air- and spaceborne data, i.e., without direct access to the glacier, to infer glacier mass changes based on a statistical relation between the equilibrium line altitude and the glacier-wide SMB (e.g., Kulkarni, 1992; Dyurgerov, 1996; Rabatel et al., 2005). These methods were applied to glaciers located in a wide range of different regions, such as in Europe (e.g., Hock et al., 2007; Rabatel et al., 2008, 2016), South America (e.g., Rabatel et al., 2012), New Zealand (e.g., Chinn, 1995, 1999), the Arctic

(e.g., Mernild et al., 2013), the Himalayas (e.g., Kulkarni et al., 2004, 2011) and Central Asia (e.g., Dyurgerov et al., 1994; Kamniansky and Pertziger, 1996). Some pioneer studies (e.g., Østrem, 1973, 1975; Young, 1981; Dyurgerov et al., 1994) have identified the value of transient snowline (TSL) observations in connection with subseasonal SMB. Recent studies (e.g., Hock et al., 2007; Pelto, 2010; Pelto et al., 2013; Huss et al., 2013; Hulth et al., 2013) have further developed this concept to improve surface mass balance monitoring and modelling strategies, including information extracted from continuous TSL observations. However, most approaches still rely on long-term glaciological information and are thus not applicable to unmonitored glaciers located in remote and unmeasured regions.

In this study, three pillars of a multi-level strategy for glacier observation are combined, covering the period of the past two decades, to improve the understanding of mass change evolution of Abramov, Golubin and Glacier No. 354, three benchmark glaciers in the Tien Shan and Pamir-Alay. (1) We integrate in situ glaciological measurements, when available, to compute annual SMB using a model-based extrapolation of the measurement points to reach glacier-wide coverage. (2) We calculate geodetic mass changes based on high-resolution digital elevation models (DEMs) on decadal to semi-decadal time scales. (3) We infer daily SMB series using a model approach supported by transient snowline observations, as a proxy for glacier mass balance. In this way, a temperature-index model is calibrated with the snow-covered area fraction (SCAF) of the glacier observed on satellite optical imagery and time-lapse photographs throughout the ablation season. This approach represents a new tool for glacier observation at high temporal and spatial resolution. The remote snowline observations provide valuable information, especially for periods for which no direct measurements are available. By combining different independent approaches, we aim to overcome the limitations and shortcomings of each individual method and to deliver a robust mass balance estimate for the three selected glaciers at annual resolution for a period for which only limited data has been available so far.

2 Study Site and Data

2.1 Study sites

In this section we present a brief overview of the study sites. A detailed description of the three selected glaciers and their geographic and climatological settings is given in Hoelzle et al. (2017). Table 1 summarizes the available data for each glacier.

2.1.1 Abramov Glacier

Abramov Glacier (N $39\,°36.78'$, E $71\,°33.32'$) is located in the Pamir-Alay (North-Western Pamir, Fig. 1). The north to northeast facing glacier has an extent of about $24\,km^2$ (as of 2016) and ranges from 3650 m a.s.l. to nearly 5000 m a.s.l. Barandun et al. (2015) suggested that the glacier had a mean annual balance of $-0.44\pm0.10\,m$ w.e. yr^{-1} between 1968 and 2014 and estimated internal accumulation and basal ablation to contribute by $+0.07\,m$ w.e. yr^{-1} to the total mass change of the glacier. Brun et al. (2017) indicated a mass loss of $-0.38\pm0.10\,m$ w.e. yr^{-1} for Abramov from ca. 2002 to 2014.

Mean daily air temperature and total daily precipitation sums were measured at a glaciological station located at 3837 m a.s.l. from 1967 to 1998 (Fig. 1). The station was located at a distance of about 0.5 km from the glacier tongue. Air temperature
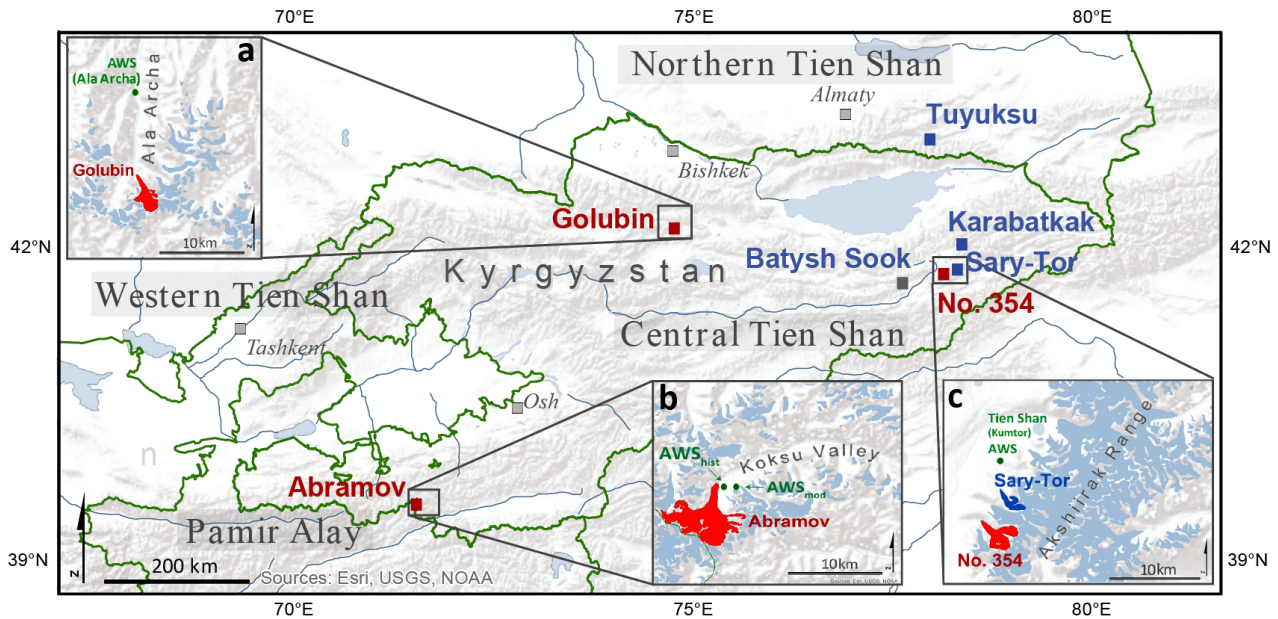
Figure 1. Overview map of Central Asia showing the location of glaciers (blue) with available long-term SMB measurements. Glaciers investigated in this study are marked in red. The insets show the position of the automatic weather station (AWS) for (**a**) Golubin, (**b**) Abramov and (**c**) Glacier No. 354. Note that AWS_{mod} indicates the position of the new AWS installed in 2011 and AWS_{hist} the old glaciological station at Abramov.

measured at an Automatic Weather Station (AWS_{mod}) was used from 2011 to 2016 (Fig. 2a). This station is located at an elevation of 4100 m a.s.l. at a distance of about 1.5 km from the glacier terminus. ERA-interim Reanalysis data with spatial resolution of 0.78 degrees (Dee et al., 2011) were used to fill measurement gaps (Barandun et al., 2015).

The SMB was measured intensively from 1967 to 1998 (Suslov et al., 1980; Glazirin et al., 1993) and the monitoring was re-established in 2011 (Hoelzle et al., 2017). Since then, annual glaciological surveys were continuously carried out in late August. For a re-analyzed and reconstructed mass balance series for Abramov from 1968 to 2014 and a detailed description of the measurement network, see Barandun et al. (2015).

2.1.2 Golubin Glacier

Golubin Glacier (N42°26.94′, E 74°30.10′) is located in the Ala Archa valley in the Kyrgyz Ala-Too in the Northern Tien Shan (Fig. 1). The glacier has an area of ∼5 km^2 (as of 2016) and a north to northwestern aspect. The terminus is currently located at an elevation of about 3400 m a.s.l. and the glacier extends to an elevation of about 4300 m a.s.l. Long-term measurements indicated an internal accumulation due to refreezing of meltwater of about +0.08 m w.e. yr^{-1} (Aizen et al., 1997). For Golubin,

the geodetic mass loss reported by Bolch (2015) was -0.28 ± 0.96 m w.e. yr^{-1} from 2000 to 2012, whereas Brun et al. (2017) found a geodetic mass balance of -0.04 ± 0.19 m w.e. yr^{-1} for the period 2002 to 2013.

We used meteorological data from the Alplager station located in the Ala Archa valley, situated at an elevation of 2145 m a.s.l. at a distance of about 10 km from the glacier (Fig. 1). There are several other meteorological stations in the valley, however, the Alplager station has the most complete and continuous series at high elevation covering the entire study period.

Intense glacier monitoring started in 1958 and continued until 1994 when the monitoring programme was stopped (Aizen, 1988). In summer 2010, SMB measurements were re-initiated. Figure 2b summarizes the monitoring network at Golubin as of 2016, including a SMB measurement network, an AWS ($\approx$3300 m a.s.l.) and two terrestrial cameras installed in 2013. A detailed description of the monitoring strategy is provided in Hoelzle et al. (2017).

2.1.3 Glacier No. 354

Glacier No. 354 (N $41°47.62'$, E $78°9.69'$) is situated in the Ak-shiirak range in the Central Tien Shan (Fig. 1). The glacier covered a surface area of about 6.4 km^2 in 2016. The accumulation zone comprises three basins and the glacier tongue is oriented to the northwest. The glacier spans an elevation range of 3750-4680 m a.s.l. Mass loss since the mid-1970s was reported by different studies ranging from about -0.8 to -0.5 m w.e. yr^{-1} (Pieczonka and Bolch, 2015; Kronenberg et al., 2016; Brun et al., 2017). Summer snowfall is frequent and fresh snow can cover the entire glacier surface for several days during the melt season, significantly reducing ablation (Kronenberg et al., 2016). Evidence of persistent superimposed ice is found and Kronenberg et al. (2016) estimated internal accumulation to be $+0.04$ m w.e. yr^{-1}. An AWS (Tien Shan (Kumtor) AWS) installed at an elevation of $\approx$3660 m a.s.l. and a distance of approximately 10 km to the glacier recorded continuous meteorological data for the study period (Fig. 1). We used daily precipitation sums and mean daily air temperature for modelling.

Since 2010, in situ SMB has been obtained annually in late summer (Fig. 2c). Winter measurements exist for May 2014 (Kronenberg et al., 2016). A description of the meteorological input data and the SMB measurement network, as well as a reconstruction of the mass balance series back to 2003 are provided by Kronenberg et al. (2016).

2.2 High-resolution satellite images and DEMs

To compute geodetic mass balances for Abramov, high-resolution DEMs were used based on Pléiades stereo images acquired in 2015, and on stereo images from 2003 and 2011 from Satellite Pour l'Observation de la Terre (SPOT) 5. For Glacier No. 354, DEMs from 2003 (QuickBird) and from 2012 (GeoEye) were available from Kronenberg et al. (2016). In addition, a SPOT6 stereo-pair acquired in 2015 was used to produce an updated DEM. High-resolution stereo images for Golubin are sparse and we had to rely on a SPOT7 tri-stereo scene from November 2014 and on Advanced Land Observing Satellite (ALOS) Prism scenes from 2006 (Table 1). Important snow coverage was present on the SPOT5 image from 2011 for Abramov and on the SPOT7 image from 2014 for Golubin. A fine layer of fresh snow covered parts of the SPOT6 image from 2015 for Glacier No. 354. For modelling purposes, the most complete and accurate DEM available of each glacier was used to represent the surface topography (Table 1).
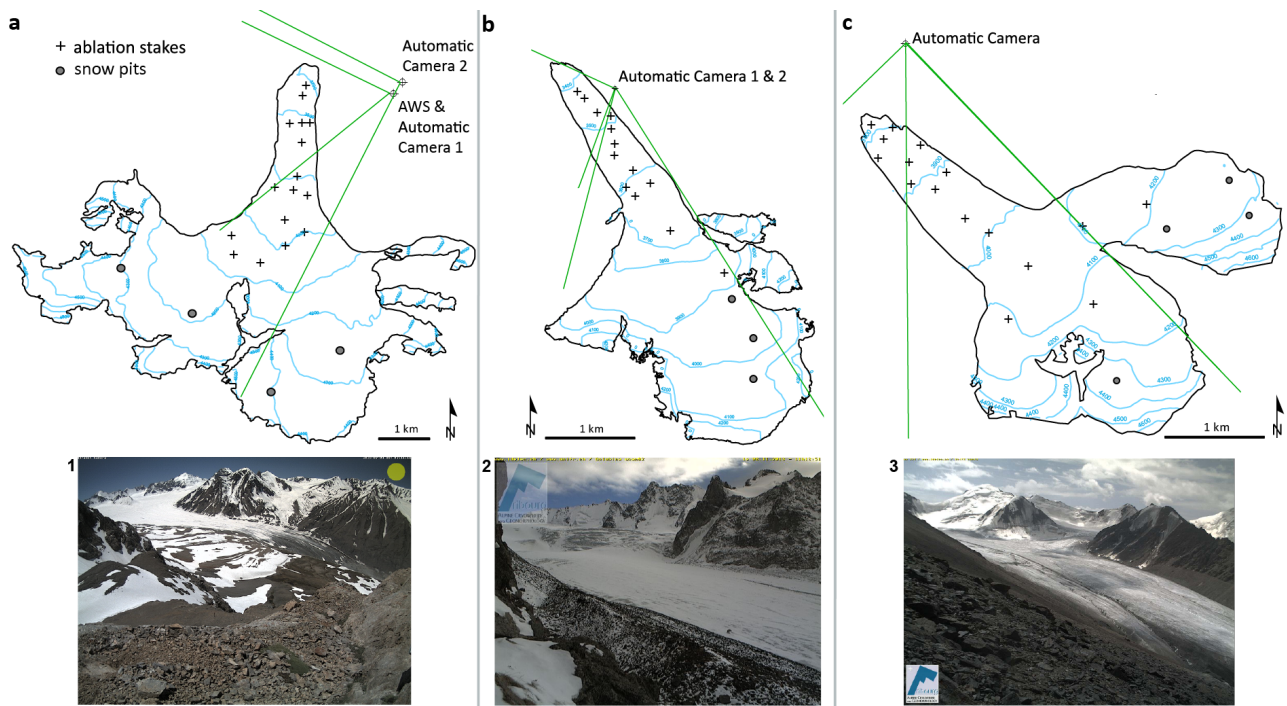
Figure 2. Glacier monitoring network at (**a**) Abramov, (**b**) Golubin and (**c**) Glacier No. 354. A photograph taken by the terrestrial cameras is shown for (**1**) Abramov, (**2**) Golubin and (**3**) Glacier No. 354.

2.3 Optical satellite and terrestrial camera images

We used freely accessible, orthorectified and georeferenced Landsat TM/ETM+ and OLI, Terra ASTER-L1B and Sentinel-2A scenes to repeatedly observe the glacier outlines and the snowline throughout the melting season for all three glaciers. In addition, we used the snow-free high-resolution optical satellite images as described above for snowline and glacier outline mapping.

Two terrestrial cameras (Mobotix M25) overlooking Abramov were installed in August 2011. One camera was located next to the $\mathrm{AWS_{mod}}$, and the other one at approximately $500\,\mathrm{m}$ distance at an elevation of $4200\,\mathrm{m}$ a.s.l. (Fig. 2a). Due to multiple camera failures and power supply problems, pictures were lacking from the end of the ablation season in 2012 to the end of the ablation season in 2013, and again partly for the summer months in 2014. In 2015, continuous coverage was obtained from Camera 1 but only a few images could be retrieved from Camera 2. A complete set of data was collected from both cameras for the first time in 2016. A similar setup has been installed for Glacier No. 354 in 2014, delivering continuous coverage since implementation (Fig. 2c). The camera is located at an elevation of $4145\,\mathrm{m}$ a.s.l. Images from the two cameras installed at Golubin were not used here due to limited image quality (Fig. 2b). Figure 3 illustrates the number of camera and satellite

Table 1. Available data on glacier monitoring for the three glaciers used in this study. The dates marked with an asterisk indicate the DEMs used as a topographic base for the modelling.

	Abramov	Golubin	Glacier No. 354
No. surface mass balance measurements per year	22	14	16
No. annual glaciological surveys (2000-2016)	5	6	6
Total No. snowline observations	122	56	78
High-resolution satellite stereo images	27/08/2003 (SPOT5)	08/09/2006 (ALOS)*	01/09/2003 (QuickBird)
	29/11/2011 (SPOT5)	01/11/2014 (SPOT7)	27/07/2012 (GeoEye)*
	01/09/2015 (Pléiades)*		01/10/2015 (SPOT6)

images with satisfying quality that were used to obtain maps of snowlines for the three glaciers. Image availability for snowline mapping prior to 1998 was insufficient for the most part.
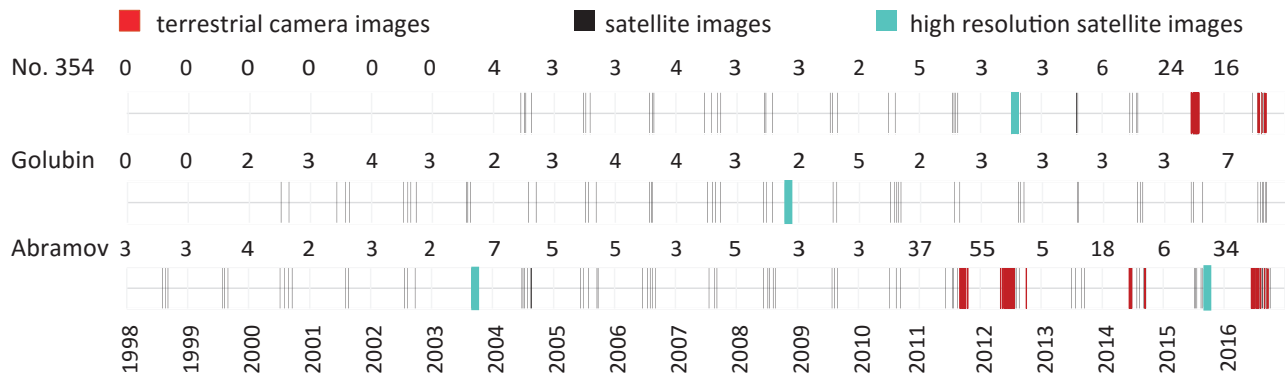
Figure 3. Image availability and distribution for snowline mapping. Numbers indicate the total available scenes per year and glacier. Prior to 1998, image coverage is sparse for all three glaciers. For Golubin and for Glacier No. 354, the first summer season for which enough snowline observations could be collected was 2000 and 2004, respectively. Snow-covered high-resolution images have not been used to delineate the snowline and are not shown here.

3 Methods

3.1 Glacier outlines

5 Glacier extents were mapped manually based on satellite images for all three glaciers and for each year of the corresponding study period. Only cloud- and snow-free images were selected. The surfaces of Glacier No. 354 and Golubin are mostly debris-free. We excluded a debris-covered part with strongly reduced melt rates at the western margin of Abramov (Barandun et al.,

2015). Annually repeated measurements of the glacier front position using a handheld GPS for all three glaciers were combined with the satellite observations for mapping from 2011 onward. The same extents were used for all three methods. Errors related to glacier outlines digitized manually on remote sensing images depend on atmospheric and topographic corrections, shading, glacier surface characteristics, snow cover and local clouds, but mainly on misinterpretation of debris cover (Paul et al., 2013,

5 2015). Uncertainties are expected to be in the range of ±5% of the total glacier area for medium-resolution images such as Landsat TM, and smaller for high-resolution images (Paul et al., 2013).

3.2 Meteorological data

For Abramov, the air temperature data measured at the AWS was adjusted to the elevation of the former glaciological station by applying a constant lapse rate of $-6\,^{\circ}\mathrm{C}\,\mathrm{km}^{-1}$ (Suslov et al., 1980). The ERA-interim Reanalysis dataset was adapted by

10 applying mean monthly additive and multiplicative biases for air temperature and precipitation, respectively. The biases were calculated from long-term in situ measurements (Barandun et al., 2015). From the corrected monthly means, daily series were generated by superimposing day-to-day variability, observed at the meteorological station from 1969 to 1994. For Abramov, we generated air temperature series from 1995 to 2011 and precipitation series from 1995 to 2016. More detailed information on data preparation and their suitability is given in Barandun et al. (2015).

15 Mean daily air temperature data measured at the Ala Archa AWS and Tien Shan (Kumtor) AWS were extrapolated to the median elevation of the corresponding glacier with monthly temperature lapse rates for the Northern and Central Tien Shan provided in Aizen et al. (1995).

3.3 Snowline delineation

A visual pre-selection of suitable camera and satellite images was taken in order to preclude problems associated with image

20 quality such as fresh snowfall, extensive cloud cover, among others. Oblique ground-based photographs were first corrected automatically for lens distortion, then projected and orthorectified following Corripio (2004). Every pixel on the photograph was associated to the elevation of the DEM. Georeferenced products of satellite scenes were downloaded. On each camera and satellite image, the snow-covered area was digitized manually by means of visual separation of bare ice and snow (Pelto et al., 2013; Mernild et al., 2013; Huss et al., 2013). Manual detection allowed the observer's knowledge of the snow-cover depletion

25 patterns to be integrated, and was assumed to be less error-prone than an automatic classification (Huss et al., 2013; Rabatel et al., 2013).

Errors occurred due to the pixel size of the images, slope of the terrain, the accuracy of the georeferencing and the quality of the DEM (Rabatel et al., 2012). In view of the fact that the border between ice and snow is not a clearly defined line, operator expertise is desired and beneficial. Contrast becomes rather weak, especially when the snowline rises above the firn

30 line (Rabatel et al., 2013; Wu et al., 2014) for both satellite and terrestrial camera images. In order to estimate the influence of ambiguous transition areas, we conducted extensive experiments on the interpretation of the surface type (see Section 4).

We assumed the spatial depletion pattern to be approximately constant in time so that camera and satellite images with minor invisible sections of the snowline due to shading, cloud cover, Landsat 7 SLC-off void-stripes or due to the terrestrial camera

Table 2. Survey period of glaciological measurement for each glacier and each year

Abramov	Golubin	Glacier No. 354
	10/09/2010–17/08/2011	05/09/2010–12/08/2011
26/08/2011–22/08/2012	17/08/2011–29/08/2012	12/08/2011–14/08/2012
22/08/2012–15/08/2013	29/08/2012–25/08/2013	14/08/2012–23/07/2013
15/08/2013–18/08/2014	25/08/2013–17/08/2014	23/07/2013–03/09/2014
18/08/2014–27/08/2015	27/08/2014–09/08/2015	03/09/2014–14/08/2015
27/08/2015–01/08/2016	09/08/2015–14/09/2016	14/08/2015–29/08/2016

view angle could be included. To fill in those data gaps, we extrapolated the snowline based on information from repeated snowline observations of images with good quality over a ≈15-year period. The effect of a misinterpretation of the snowline on the calculated SMB was investigated in detail and is described in Section 4.

3.4 Glaciological surface mass balance

5 Ablation stakes are distributed over the entire ablation zone in order to provide an optimal representation of melt patterns (Fig. 2). Each year, they are re-drilled at the initial position. An ice density of $900\,\mathrm{kg\,m^{-3}}$ was assigned. Snow pits were dug to the previous end-of-summer horizon to measure snow density and snow accumulation. Annual field surveys ranged from late July to late August and for logistic reasons, can vary from year to year. Winter snow measurements were carried out to retrieve a detailed snow distribution pattern, and to compute the winter balance for Glacier No. 354 and Golubin in

10 May 2014 (Kronenberg et al., 2016). Winter surveys from 1993 and 1994 were available for Abramov (Pertziger, 1996). A model-based spatial extrapolation of point measurements to the entire glacier surface after Huss et al. (2009) was used to retrieve glacier-wide SMB for all years with direct measurements. The model is a combined distributed accumulation (Huss et al., 2008) and temperature-index melt model with daily resolution (Hock, 1999) which was automatically optimized to best represent all collected point data from each seasonal/annual survey. The model is considered as a suitable tool to extrapolate

15 the glaciological point measurements to the glacier surface for the measurement periods.

3.5 Geodetic mass balance

For Abramov, the 4-m Pléiades DEM from 1 September 2015 was used as reference. It was created using the AMES stereo-pipeline (Shean et al., 2016) and the processing parameters that were used in Marti et al. (2016). The two SPOT5 DEMs (August 2003 and November 2011) were derived from High Resolution Stereoscopic (HRS) images by the French mapping

20 agency (Korona et al., 2009). The steps required to adjust the two SPOT5 DEMs horizontally and vertically to the Pléiades reference DEM are similar to the ones followed in a previous study on the Mont Blanc area (Berthier et al., 2014).

We created DEMs with a spatial resolution of 5 m for Golubin and Glacier No. 354 from the available two/tri-stereo pairs of high-resolution satellite imagery using standard procedures and the software PCI Geomatica (Kronenberg et al., 2016). The

two/tri-stereo pairs were connected using common tie points before DEM extraction. For Glacier No. 354, a horizontal shift between the two DEMs was corrected through a DEM co-registration procedure as proposed by Nuth and Kääb (2011). For the data covering Golubin, no horizontal shift was encountered. We thus corrected only for a mean elevation difference of 3.9 m detected over stable ground. For this vertical co-registration, only terrain sections with a slope smaller than 30° were selected and areas with parallax-matching problems were avoided. Snow-covered areas were included in the offset correction, in order to correct for fresh snow on the image, assuming similar snow thicknesses on- and off-glacier. The vertical accuracy was thus improved, and the mean absolute difference off-glacier was limited to 1.0 m (2003-2015) and 0.6 m (2011-2015) for Abramov, 0.7 m for Glacier No. 354 and 1.6 m for Golubin (see also Section 4). Steep mountain walls and shading caused problems. Areas affected were manually masked out. Unmeasured areas (Abramov: 26% in 2003-2015, and 23% in 2011-2015; Golubin: 30%; Glacier No. 354: 25%) were assumed to have experienced the same elevation change as the measured areas in the same altitude band and the median of the corresponding elevation bin was used for gap-filling. For elevation bins higher than 4300 m a.s.l. at Golubin (9% of total area) and for elevation bins higher than 4500 m a.s.l. at Glacier No. 354 (8% of total area), obvious DEM errors were dominant and not enough realistic values for median elevation-change calculation were available. Thus, the median of the uppermost elevation band with reliable data was used to fill in the gaps. To derive the geodetic mass balance ΔM_{geod}, a density $\rho_{\Delta \mathrm{V}}$ of 850 kg m^{-3} was used for volume-to-mass conversion (Huss, 2013):

$$\Delta M_{\mathrm{geod}} = \frac{\Delta V \cdot \rho_{\Delta \mathrm{V}}}{\overline{A} \cdot \Delta t} \tag{1}$$

where, $\overline{A}$ is the average glacier area and Δt is the time in years between the corresponding image pairs. Uncertainties in the detected elevation changes and the derived geodetic mass balances are described in Section 4.

3.6 Surface mass balance modelling constrained by snowline observations

An accumulation and temperature-index melt model closely constrained by transient snowline observations was implemented in order to infer glacier-wide SMBs. The applied methodology is a further stage in the approach presented by Huss et al. (2013). The principle of the approach is to employ the information given by the temporal change in the position of the transient snowline throughout the ablation season to constrain both the amount of winter snow accumulation and melting by iteratively calibrating a mass balance model. The approach also allows us to temporally extend SMB estimates to the end of the hydrological year although snowline observations do not cover the entire ablation season. The methodological steps are described in more detail in the following.

A surface mass balance model with a spatial resolution of 20 m was driven with daily mean air temperature and precipitation sums measured at nearby meteorological stations or inferred from Reanalysis data (see Section 2.1). We used a classical

temperature-index melt model (e.g., Braithwaite, 1995; Hock, 2003). Melt M was calculated for each grid cell x, y and time step t based on a linear relation with positive daily mean air temperature $T_{\mathrm{air}}(x, y, t)$ as

$$
M_{x,y,t} = \begin{cases} DDF_{\mathrm{ice/snow}} \cdot T_{\mathrm{air(x,y,t)}} & T_{\mathrm{air}} > 0° \\ 0 & T_{\mathrm{air}} \leq 0° \end{cases} \tag{2}
$$

Daily air temperatures are extrapolated to each grid cell using a constant temperature lapse rate based on literature values (Table 3). Different degree-day factors $DDF_{\mathrm{ice/snow}}$ were chosen for snow and ice surfaces. The surface type over the glacier area was given by the snow depth updated with modelled daily snowfall and melt. The ratio between DDF_{ice} and DDF_{snow}, R_{DDF}, was held constant over time. As a wide range of different ratios can be found in literature (e.g., Hock, 2003; Zhang et al., 2006; Gao et al., 2010; Liu and Liu, 2016), we decided to constrain R_{DDF} by SMB measurements in the Tien Shan and Pamir (Table 3). A sensitivity test shows that a variation of R_{DDF} by $\pm 25\%$, a value exceeding the maximum range found in the literature ($\pm 22\%$), only causes small changes in modelled SMB (Table 4) indicating that calibrating R_{DDF} improves model performance to some extent but is not essential to applying the model. For more details see Section 4.

Snow accumulation C was calculated for each grid cell x, y and time step t by

$$
C_{(x,y,t)} = P_{\mathrm{ws}}(x, y, t) \cdot C_{\mathrm{prec}} \cdot (1 + (z_{(x,y)} - z_{\mathrm{ws}}) \cdot \delta P / \delta z), \tag{3}
$$

where P_{ws} is the measured precipitation at the meteorological station at elevation z_{ws}. $z(x,y)$ is the elevation of each grid cell. The measured precipitation was extrapolated to every grid cell with a constant precipitation gradient $\delta P / \delta z$ calculated from winter snow surveys (Table 3). Solid precipitation occurs at $T_{\mathrm{air}} \leq 1.5\,°C$ with a linear transition range of $\pm 1°C$ (e.g., Hock, 1999). C_{prec} is a scaling factor that accounts for gauge under-catch and other systematic measurement errors of precipitation (e.g., Huss et al., 2009). In order to account for smaller measurement errors during summer related to the type of precipitation (solid/liquid, wet/dry snow), C_{prec} was reduced for the summer months to 25% of its value (Sevruk, 1981). Above a critical elevation Z_{crit}, precipitation is set to no longer increase linearly (Alpert, 1986). Our selected value of Z_{crit} approximated the elevation for which a decrease in accumulation was observed on long-term monitored glaciers situated in the Tien Shan and Caucasus (WGMS, 2013). All parameters used are summarized in Table 3.

3.6.1 Model calibration

We calibrated C_{prec} and DDF_{snow}, keeping R_{DDF} constant. C_{prec} and DDF_{snow} were calibrated annually and for each glacier separately to correctly represent the winter snow accumulation and the melt rate. To calibrate C_{prec}, we relied on the fact that, at the position of the transient snowline, icemelt had not yet started but all winter snow was melted. The modelled cumulative melt, calculated at the position of the observed snowline, is thus interpreted as the total amount of accumulated winter snow that melted from the onset of the ablation season until the snowline observation date. Using the melt model, we can infer the winter accumulation at the beginning of the ablation season along each observed snowline. This quantity needs to agree with

Table 3. Constant model parameters. The temperature lapse rate for Abramov was adopted from Barandun et al. (2015) and for Golubin and Glacier No. 354 from Aizen et al. (1995). $\delta T/\delta z$, $\delta P/\delta z$, Z_{crit} and R_{DDF} are held constant throughout the entire modelling period. The initial parameter ranges of DDF_{snow} and C_{prec} as well as the mean value obtained from annual calibration is given with its standard deviation.

parameter	Abramov	Golubin	Glacier No. 354	unit
$\delta T/\delta z$	-4.8	-6.3	-6.7	$^\circ$C km^{-1}
$\delta P/\delta z$	6.4	4.5	1.5	% 10^{-4} m^{-1}
R_{DDF}	1.57	1.36	1.06	–
Z_{crit}	4400	4000	4500	m a.s.l
annually variable model parameters				
initial range				
DDF_{snow}	$3.5-5.5$	$3.0-5.5$	$1.5-4.5$	mm day^{-1} $^\circ$C^{-1}
C_{prec}	$1.75-3.0$	$1.5-3.0$	$1.0-3.5$	–
best combination				
DDF_{snow}	4.54 ± 0.74	5.09 ± 0.46	3.04 ± 0.66	mm day^{-1} $^\circ$C^{-1}
C_{prec}	2.23 ± 0.40	1.46 ± 0.31	2.35 ± 0.29	–

the directly modelled snow accumulation at the end of the winter season. DDF_{snow} was calibrated to best represent all SCAF observations of one ablation season (Fig. 4).

As C_{prec} and DDF_{snow} depend on each other, overestimation of DDF_{snow} could cause an overestimation of C_{prec}, and vice versa, without affecting the modelled position of the snowline and the SCAF. To overcome this problem, the values of C_{prec} and DDF_{snow} were constrained to remain within realistic bounds. Through an iterative calibration procedure, we aimed at finding the best possible parameter combination without the need of any additional information.

First, we defined a plausible range for DDF_{snow} and C_{prec} for all three glaciers based on literature (Hock, 2003; Liu and Liu, 2016) (Table 3). For each DDF_{snow}, an optimal parameter C_{prec} was calibrated through iteratively narrowing a plausible range of initial values of C_{prec} (Fig. 4). In this way, the RMSE between the directly modelled winter snow accumulation $Accu_{modelled}$ and the modelled cumulative melt from the onset of the ablation season to each observation date $Melt_{modelled}$ was minimized until no further improvement of the RMSE was observed.

Second, the performance of each DDF_{snow} with its optimal C_{prec} pair, was evaluated based on the RMSE$_{SCAF}$ between the observed $SCAF_{obs}$ and the modelled $SCAF_{modelled}$ for all available snowline observations within one year (Fig. 4). The range of DDF_{snow} was narrowed around the best solution and the optimization process was restarted until no further significant improvement of the RMSE$_{SCAF}$ was observed. The calibration procedure was repeated for each year individually.

A minimum of two images was needed to enable application of our calibration approach. The influence of the image frequency and distribution was assessed in detail with sensitivity experiments described in Section 4. In a last step, the calibrated model was re-run with the ideal parameter set. This snowline-constrained mass balance model was thus applied to derive con-
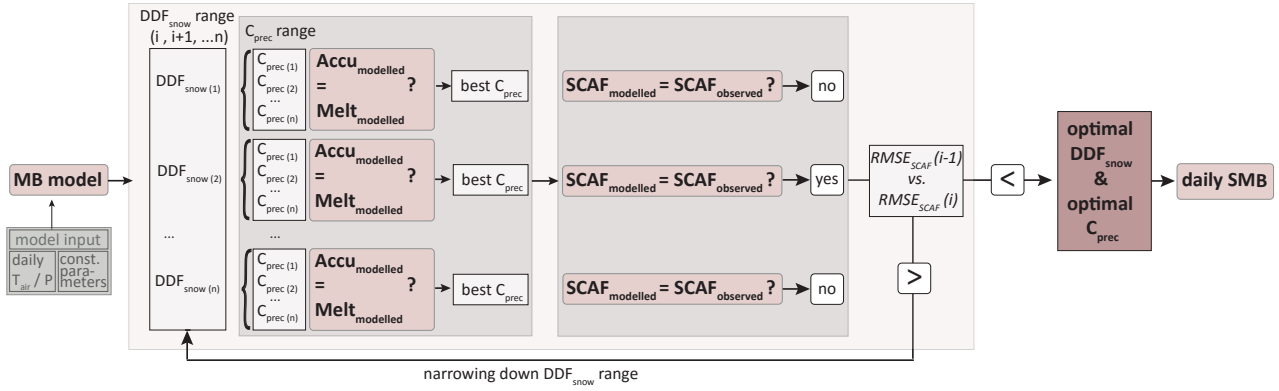
Figure 4. Calibration procedure to obtain an ideal combination of DDF_{snow} and C_{prec}. An initial range for DDF_{snow} and C_{prec} was narrowed down through comparison to snowline observations until an optimal solution for both parameters was found. First, for each initial value of DDF_{snow}, the best value of C_{prec} was determined constraining the modelled cumulative melt ($Melt_{\mathrm{modelled}}$) at the snowline position to agree with the modelled winter snow accumulation ($Accu_{\mathrm{modelled}}$) for the same location. Second, the performance of each DDF_{snow} was evaluated to narrow down the range of DDF_{snow} by comparing the RMSE$_{\mathrm{SCAF}}$ of the modelled and observed snow-covered area fractions (SCAF). This was repeated until an optimal solution is reached.

tinuous daily SMB series that agreed with the snow depletion patterns observed by remote sensing imagery. In the following, we refer to the methodology described above as *snowline approach*.

3.6.2 Adjustments to enable comparison of different methods

Geodetic surveys provide an estimate of the total mass change of a glacier ΔM_{geod}, whereas the results inferred from the snow-
5 line approach refer to the surface mass balance B_{sfc} and do not account for internal and basal components of the mass balance (Cogley et al., 2011). For comparing the results, we adjusted the modelled SMB constrained by snowline observations, with an estimate of the internal/basal mass balance of $+0.07\,\mathrm{m\,w.e.\,yr^{-1}}$ for Abramov (Barandun et al., 2015), $+0.08\,\mathrm{m\,w.e.\,yr^{-1}}$ for Golubin (Aizen et al., 1997) and $+0.04\,\mathrm{m\,w.e.\,yr^{-1}}$ for Glacier No. 354 (Kronenberg et al., 2016). Values are positive due to a significant amount of refreezing of meltwater in cold firn.
10 To compare the results of the different methods, the time periods covered by the datasets also needed to be homogenized. We thus adjusted the observation period of the modelled mass balance constrained by snowline observations to exactly match the respective periods of geodetic and glaciological mass balance, respectively. However, the final results $B_{\mathrm{sfc(fix)}}$ derived from the snowline approach are presented for the fixed dates of the hydrological year (1 October to 30 September) and do not include internal/basal mass balance.

4 Uncertainties and model sensitivity

4.1 Glaciological surface mass balance

Uncertainty σ_{glac} related to the direct glaciological measurements for Abramov was adopted from Barandun et al. (2015), and for Glacier No. 354 from Kronenberg et al. (2016). Uncertainties concerning the SMB of Golubin were calculated after Kronenberg et al. (2016). Uncertainties regarding all three glaciers range between 0.24 and 0.30 m w.e. yr^{-1} (Table 4). For a sensitivity experiment we artificially shifted temperature and precipitation series used for the model-based extrapolation by $\pm 1°$C and $\pm 25\%$, respectively. The resulting glacier-wide SMB indicate a very small sensitivity to the meteorological input data with a Standard Deviation (STD) of <0.01 mm w.e. yr^{-1}. We strictly refer to the annual SMB obtained for the measurement dates (table 2).

4.2 Geodetic mass balance

The total uncertainty of the geodetic mass balance includes a random and systematic error. We followed Brun et al. (2017) for computing the random error of the geodetic mass balance estimate but did not assess the systematic error. Uncertainties in elevation differences were quantified by computing the area-weighted mean of the absolute difference off-glacier in 50 m altitude bins. The resulting values for Abramov, 1.0 m for 2003-2015 and 0.6 m for 2011-2015, and for Glacier No. 354, 0.7 m for 2012-2015, are in line with the uncertainty of 1.3 m found over the Mont Blanc area through comparison of similar satellite data to elevation differences measured in situ (Berthier et al., 2014). For Golubin, a value of 1.6 m indicates a slightly lower DEM quality. The uncertainty related to the density assumption for converting volume to mass change was assumed to be ± 60 kg m^{-3} for time intervals larger than five years (Huss, 2013). For shorter periods, we used a more conservative estimate of ± 120 kg m^{-3}. The elevation uncertainty for unmeasured glacier zones was roughly estimated to be five times as large as the uncertainty determined for measured locations. We assumed independence between the different error components and combined them as Root-Sum-Square (RSS) to the total uncertainty for the geodetic mass balance, σ_{geod}.

4.3 Surface mass balance modelling constrained by snowline observations

The uncertainty introduced by the mass balance model constrained by transient snowline observations σ_{tsl} depends on (1) the delineation accuracy of the SCAF, σ_{map}, (2) the image frequency and distribution throughout the ablation season, σ_{dis}, (3) the DEM quality, σ_{DEM}, (4) the meteorological input data, σ_{meteo}, and (5) the uncertainty in constant model parameters, σ_{para} (Table 4). The individual components were estimated as follows:

(1) The accuracy of the mapped SCAF is dependent on the positioning and the transect of the snowline, the georeferencing of the images, and the extrapolation of the snowline to invisible areas (Huss et al., 2013). The limit between snow- and ice-covered areas is often not a clear line but rather a transition zone, especially for glaciers with superimposed ice. To account for the total uncertainty related to the mapping procedure, we identified an upper- and lowermost position of the surface that could be classified as either snow or ice on each available image. Hence this zone included all ambiguous areas observed,

such as cloud-covered regions, shading, superimposed ice or invisibility due to reduced image quality (e.g., Landsat 7 SLC-off void-stripes, invisible areas on photographs). We interpreted the zone to be either entirely snow-covered or entirely snow-free. The standard deviation of the minimal, maximal and optimal SCAF was used as an uncertainty. This uncertainty was calculated for each image individually. To evaluate the corresponding effects on calculated SMB, the model was re-run with the maximal

5 and the minimal possible SCAF. The standard deviation of the SMB, σ_{map}, ranged between 0.06 to 0.09 m w.e. yr^{-1} for the three glaciers.

(2) To estimate the effect of varying image availability, we repeated the modelling using different snowline observation frequencies and temporal distributions throughout the summer for calibration. Due to limited image availability, this could only be conducted for the few years when many images were available (Fig. 3). We used the results to create a look-up

10 table that linked the image frequency, the distribution over the ablation season and the last observation date of the season to an uncertainty estimate in the calculated annual SMB, σ_{dis}. Tests showed that the model reacts more sensitively to image distribution than to reduced image frequency (Fig. 5). A minimum of two images well distributed throughout the ablation season (i.e., at the beginning/middle and at the end) is sufficient to achieve reliable SMB estimates. Greater uncertainties were found if images were concentrated on, for example, a few days at the beginning of the ablation season (Fig. 5). In this case,

15 higher image frequency cannot compensate for the missing information on the snow depletion pattern. An image taken towards the end of the ablation season is more important than images from the beginning of the summer. Our assessment of image availability resulted in smaller uncertainties for Abramov ($\sigma_{\mathrm{dis}} = 0.09$ m w.e. yr^{-1}) than for Golubin ($\sigma_{\mathrm{dis}} = 0.16$ m w.e. yr^{-1}) and for Glacier No. 354 ($\sigma_{\mathrm{dis}} = 0.18$ m w.e. yr^{-1}) (Table 4).

(3) To estimate the uncertainty caused by the DEM used for the modelling, we compared our results to those obtained from

20 model runs that used lower-resolution DEMs. For this experiment, we replaced the high-resolution DEM with the SRTM DEM. This enabled us to both investigate the sensitivity of the results to DEM quality and to assess our assumption of unchanged topography during the entire study period. The effects of a reduced DEM quality for all three glaciers were found to be small ($\sigma_{\mathrm{DEM}} < 0.03$ m w.e. yr^{-1}).

(4) We investigated the uncertainty related to the meteorological input data, σ_{meteo}, by re-running the model with a climato-

25 logical average daily temperature and precipitation series for each glacier instead of the actual meteorological series. The test assessment revealed an RMSE of 0.13 m w.e. yr^{-1} for the annual SMB of Abramov, of 0.23 m w.e. yr^{-1} for Golubin and of 0.14 m w.e. yr^{-1} for Glacier No. 354 (Fig. 6). These results demonstrate a relatively low sensitivity of our model approach to daily meteorological input data. With the chosen calibration procedure the model parameters DDF_{snow} and C_{prec} are adjusted to best represent the TSL observations for each year and glacier individually. The modelled SMB are thus closely tied to the

30 snowline observations and exhibit a reduced dependence from meteorological input data. This underline the potential of our methodology for regional application based on minimal input data.

(5) To test the uncertainty introduced by the constant (i.e. uncalibrated) model parameters, $\delta T/\delta z$, $\delta P/\delta z$ and the R_{DDF} were varied by $\pm 25\%$ for each glacier and year. A mean standard deviation, σ_{para}, of around 0.17 m w.e. yr^{-1} was found. We additionally tested the behaviour of the model relative to the individual parameters and identified a higher sensitivity to $\delta T/\delta z$

35 and R_{DDF}, whereas sensitivities to the other parameters were minor (Table 5).
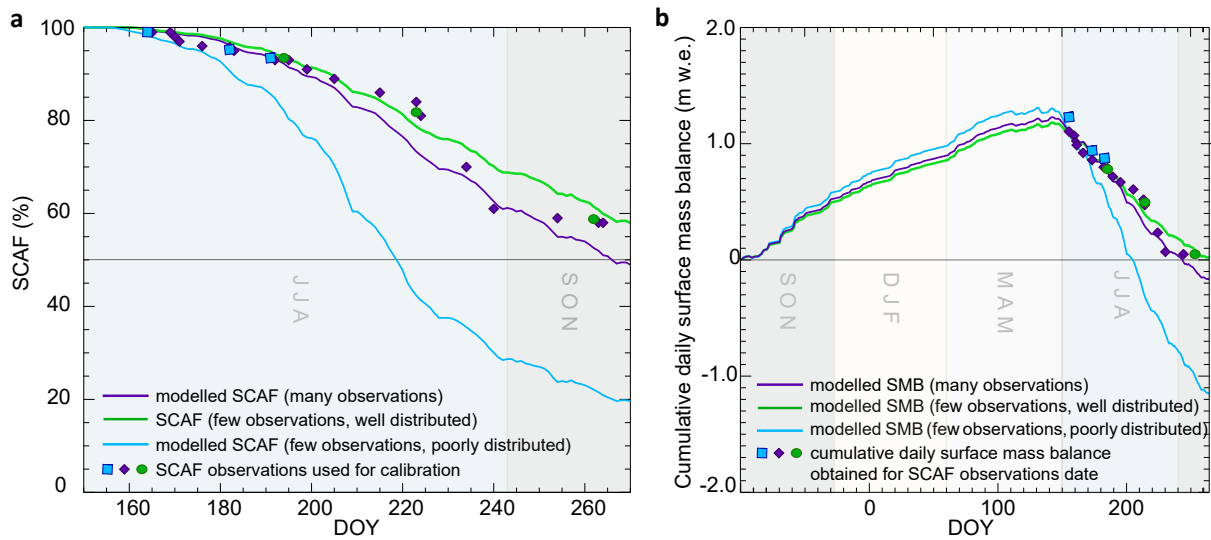
Figure 5. Example of the (**a**) daily SCAF and (**b**) cumulative daily SMB obtained with different sets of image frequency and distribution for Abramov in 2016. Snowline observation dates used to calibrate the model are indicated with symbols. The modelled daily SCAF and cumulative daily SMB and their corresponding snowline observations are shown with the same colour. Three images at the beginning of the ablation season (blue), three images well distributed throughout the ablation season (green), or all available images (purple) were used.
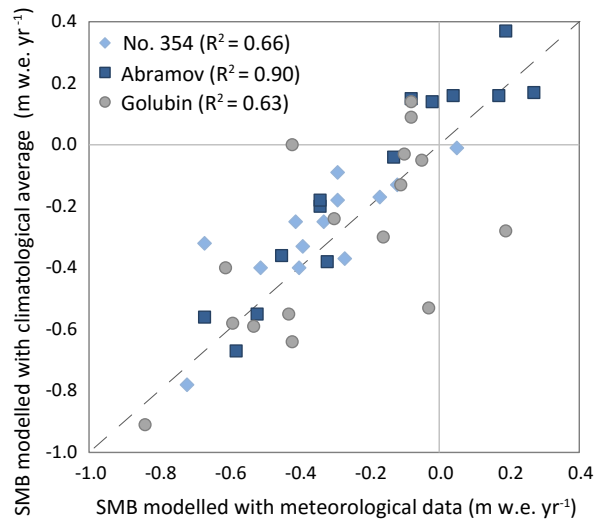
Figure 6. Comparison between the annual SMB obtained from the snowline-constrained model when using meteorological and climatological average daily data for Abramov, Golubin, and Glacier No. 354.

Table 4. Overall average uncertainties related to the three methods used, namely the glaciological σ_{glac}, geodetic σ_{geod} and snowline-constrained modelled mass balances σ_{tsl} for all three investigated glaciers in m w.e. yr^{-1}. Additionally, the uncertainty for each component of the snowline approach is specified. σ_{map} shows the uncertainty of the snowline delineation, σ_{dis} the uncertainty related to image frequency and distribution, and σ_{DEM} to the DEM. σ_{meteo} indicates the uncertainty introduced by the meteorological input data and σ_{para} the one by the model parameter choice.

Uncertainty in	Abramov	Golubin	Glacier No. 354
Glaciological SMB			
σ_{glac}	0.25	0.30	0.24
Geodetic mass balance			
σ_{geod}	0.16 (2003–15)	0.37	0.32
	0.26 (2011–15)		
SMB from snowline approach			
σ_{tsl}	0.27	0.32	0.36
σ_{map}	0.05	0.06	0.09
σ_{dis}	0.03	0.16	0.18
σ_{DEM}	0.12	0.03	0.02
σ_{meteo}	0.13	0.23	0.14
σ_{para}	0.20	0.17	0.20

Table 5. Model sensitivity to the different constant input parameters for each glacier in m w.e. yr^{-1}. See text for details on the experiments.

sensitivity in	Abramov	Golubin	Glacier No. 354
$\delta T / \delta z$	0.06	0.14	0.05
$\delta P / \delta z$	0.07	0.08	0.01
R_{DDF}	0.11	0.25	0.06

Components 1 to 5 are assumed to be independent of each other and are combined as RSS to represent the total error of the annual SMB σ_{tsl} obtained from the snowline approach. We then averaged the annual error over the different periods to compute overall uncertainty.

5 Results

5.1 Long-term surface mass balances derived from snowline approach

We found that the mass balance model constrained by snowline observations is capable of representing the observed SCAFs on satellite and terrestrial camera images within $\pm 8\%$ for Abramov, $\pm 13\%$ for Golubin and $\pm 9\%$ for Glacier No. 354 (Fig.

7). Comparing the SCAF observed on camera and on spaceborne images for the same day reveals a RMSE of 2.5%. However, tests showed that the influence of the image source (terrestrial/space-borne) on the inferred SMB is negligible.
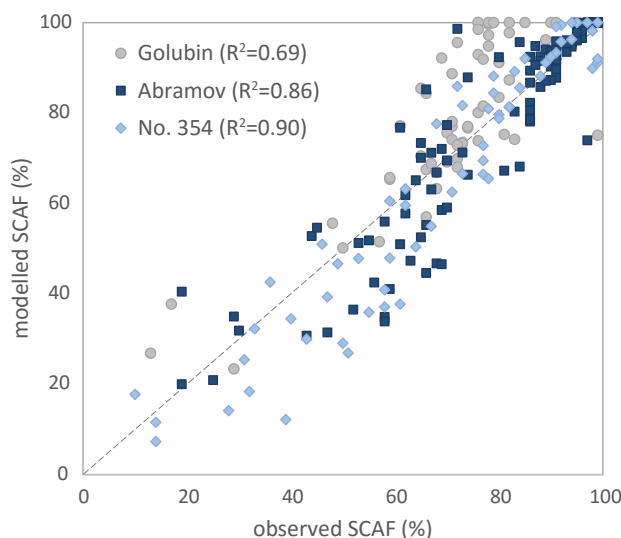
Figure 7. Comparison between observed and modelled SCAF for Abramov, Golubin, and Glacier No. 354.

Annual glacier-wide modelled surface mass balances constrained by snowline observations, calculated for Abramov (1998-2016), for Golubin (2000-2016), and for Glacier No. 354 (2004-2016), are predominantly negative (Fig. 8 and Table 6). Study periods depend on the data availability for each glacier. Abramov exhibited a mean annual SMB of -0.30 ± 0.19 m w.e. yr^{-1} from 2004 to 2016. For Golubin and Glacier No. 354 a slightly more negative annual average balance of -0.41 ± 0.33 m w.e. yr^{-1} and -0.36 ± 0.32 m w.e. yr^{-1}, respectively, was calculated for the same time period (Table 6). Length change measurements underline the observed negative balance regime of all three glaciers (Hoelzle et al., 2017). A significant glacier retreat was observed for the last century. A first speed-up of frontal retreat occurred in the 1980s and acceleration was observed in the last decade. However, no clear acceleration of mass loss for the three glaciers was identified over the investigated periods. Two phases of close-to-zero SMB could be recognized (2002-2005 and 2009-2011) for all glaciers. A lower standard deviation of annual mass balances from 2004 to 2016 is found for Glacier No 354 (0.19 m w.e. yr^{-1}) than for Golubin (0.4 m w.e. yr^{-1}) and Abramov (0.29 m w.e. yr^{-1}), which indicated higher interannual variability for the latter two. Glacier No. 354, receiving lower amounts of total annual precipitation, showed a smaller mass turnover and had a positive balance only in 2009 (Table 6). For Golubin most negative values were found in 2012 and 2014. Abramov and Golubin also had strongly negative balances in 2006 and 2008. For Abramov, the snowline observations indicated that the snowline rose close to the upper edge of the glacier already at the end of August. For Golubin, observations of the last image of the season showed that the SCAF decreased to less than 45% already in mid-August in 2006, similar to 2001 and 2015. The ablation season typically stretched until the end of September, and summer snowfalls during this month were rare (Aizen et al., 1995), likely leading to continued mass loss.

Data availability, however, was rather critical for Golubin in 2008, which is also reflected by the larger uncertainties. The last snowline observation dates from as early as the end of July.
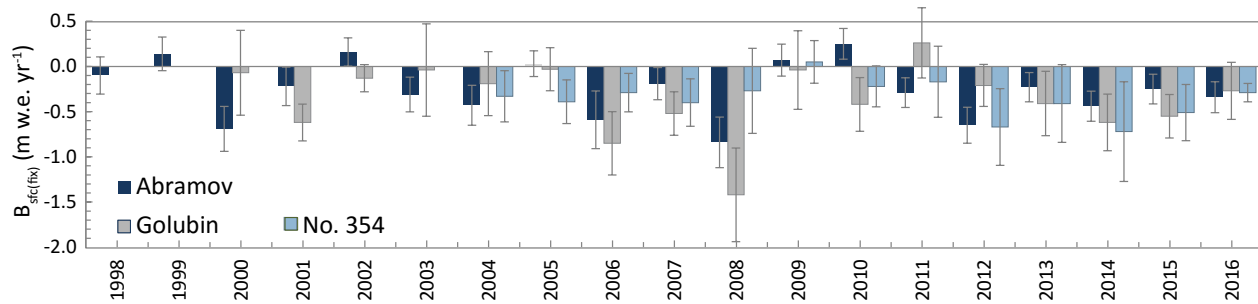
Figure 8. Modelled annual SMB $B_{\mathrm{sfc(fix)}}$ constrained by snowline observations for all three glaciers for the hydrological year.

5.2 Comparison to glaciological and geodetic mass balances

The glaciological and geodetic surveys delivered two extensive and independent datasets for validation of the modelled mass
5 balance series constrained by snowline observations. Joint analysis of the data sets permitted robust conclusions to be drawn about the mass change and its temporal dynamics over the past two decades. The glaciological SMB measurements showed a good agreement with the SMB inferred using snowline observations for the same time periods (Table 7). Exact survey dates are given in table 2. Annual glaciological SMB was reproduced with an RMSE of less than ± 0.26 m w.e. yr^{-1} for all three glaciers using the snowline approach (Fig. 9). For Golubin and Glacier No. 354, the glaciological SMB was slightly more negative than
10 the modelled SMB (Table 7). For Abramov, on the other hand, the glaciological SMB was somewhat less negative than the snowline-constrained model results. In general, a satisfactory agreement was obtained between the two methods for all three glaciers (Fig. 9). Squared correlation coefficients between snowline constrained model results and glaciological SMB ranged between r^2=0.63 (Abramov) and r^2=0.90 (Golubin).

Table 8 and Figure 10 summarize the results obtained from the different geodetic surveys. For the comparison with the
15 geodetic mass change, an estimate for internal/basal mass balance was added to the modelled SMB constrained by snowline observations (see Subsection 3.6.2) and referred to as the modelled total mass change constrained by snowline observations. The geodetic method reveals a total mass balance of -0.30 ± 0.37 m w.e. yr^{-1} for Golubin from 8 September 2006 to 1 November 2014 (Fig. 10). The corresponding total modelled mass balance constrained by snowline observations was slightly more negative with -0.38 ± 0.35 m w.e. yr^{-1} for the same period (Table 8 and Fig. 11). Comparison of digital elevation models
20 indicated that Glacier No. 354 had a mass balance of -0.58 ± 0.31 m w.e. yr^{-1} from 27 July 2012 to 1 October 2015 (Fig. 10) and -0.42 ± 0.07 m w.e. yr^{-1} from 1 September 2003 to 27 July 2012 (Kronenberg et al., 2016). The total annual mass change for the same time intervals derived from the snowline approach was -0.53 ± 0.43 m w.e. yr^{-1} and -0.25 ± 0.31 m w.e. yr^{-1}, respectively. For the first period, the results are in good agreement, whereas for the second period the mass balance model

Table 6. Annual, glacier-wide SMB for the three glaciers for the hydrological year $B_{\mathrm{sfc(fix)}}$ in m w.e. yr^{-1} inferred from the mass balance model constrained by snowline observations.

year	Abramov	Golubin	Glacier No. 354
1998	-0.10 ± 0.21		
1999	$+0.14 \pm 0.19$		
2000	-0.69 ± 0.25	-0.07 ± 0.47	
2001	-0.22 ± 0.21	-0.62 ± 0.20	
2002	$+0.16 \pm 0.16$	-0.13 ± 0.15	
2003	-0.31 ± 0.19	-0.04 ± 0.51	
2004	-0.43 ± 0.22	-0.19 ± 0.35	-0.33 ± 0.28
2005	$+0.03 \pm 0.14$	-0.03 ± 0.24	-0.39 ± 0.24
2006	-0.59 ± 0.32	-0.85 ± 0.35	-0.29 ± 0.21
2007	-0.19 ± 0.18	-0.52 ± 0.24	-0.40 ± 0.26
2008	-0.84 ± 0.28	-1.42 ± 0.52	-0.27 ± 0.47
2009	$+0.07 \pm 0.18$	-0.04 ± 0.43	$+0.05 \pm 0.24$
2010	$+0.25 \pm 0.17$	-0.42 ± 0.30	-0.22 ± 0.23
2011	-0.29 ± 0.16	$+0.26 \pm 0.39$	-0.17 ± 0.39
2012	-0.65 ± 0.20	-0.21 ± 0.23	-0.67 ± 0.42
2013	-0.23 ± 0.16	-0.41 ± 0.36	-0.41 ± 0.43
2014	-0.44 ± 0.17	-0.62 ± 0.31	-0.72 ± 0.55
2015	-0.25 ± 0.16	-0.55 ± 0.24	-0.51 ± 0.31
2016	-0.34 ± 0.17	-0.27 ± 0.31	-0.29 ± 0.10
2004-2016	-0.30 ± 0.19	-0.41 ± 0.33	-0.36 ± 0.32

Table 7. Annual SMB $B_{\mathrm{sfc(meas)}}$ for the measurement periods (i.e., exact dates of the surveys (Table 2)) based on direct glaciological measurements and on the snowline-constrained model for the three glaciers in m w.e yr^{-1}.

	Abramov		Golubin		Glacier No. 354	
year	glaciological	snowline-constrained	glaciological	snowline-constrained	glaciological	snowline-constrained
2011			-0.06 ± 0.30	-0.05 ± 0.39	-0.21 ± 0.27	$+0.34 \pm 0.39$
2012	-0.29 ± 0.30	-0.47 ± 0.20	-0.14 ± 0.30	$+0.06 \pm 0.23$	-0.52 ± 0.26	-0.74 ± 0.42
2013	-0.31 ± 0.34	-0.27 ± 0.16	-0.10 ± 0.30	-0.07 ± 0.36	-0.54 ± 0.25	-0.45 ± 0.43
2014	-0.74 ± 0.10	-0.50 ± 0.17	-1.56 ± 0.30	-1.44 ± 0.31	-0.68 ± 0.22	-0.74 ± 0.55
2015	-0.24 ± 0.25	-0.65 ± 0.16	-0.62 ± 0.30	-0.45 ± 0.24	-0.68 ± 0.24	-0.60 ± 0.31
2016	$+0.38 \pm 0.25$	$+0.24 \pm 0.17$	$+0.36 \pm 0.30$	-0.04 ± 0.31	-0.41 ± 0.24	-0.26 ± 0.10
2011-2016	-0.24 ± 0.25	-0.33 ± 0.17	-0.35 ± 0.30	-0.33 ± 0.31	-0.51 ± 0.24	-0.41 ± 0.37
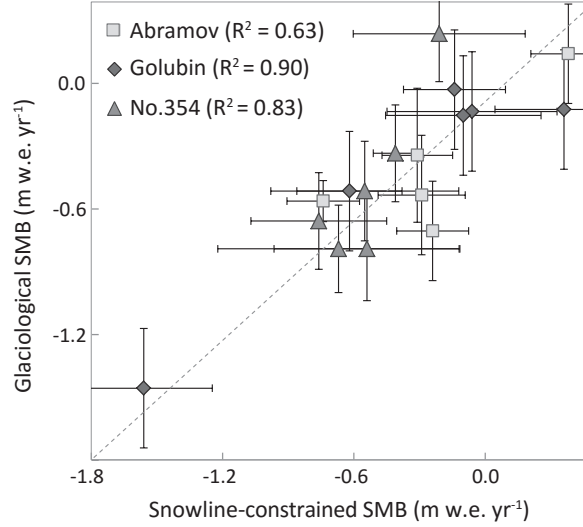
Figure 9. Comparison of modelled annual SMB constrained by snowline observations and glaciological SMB for Abramov, Golubin, and Glacier No. 354. Uncertainties in the annual SMB are indicated.

Table 8. Geodetic mass change $\Delta M_{\mathrm{geod(meas)}}$ and the total annual mass change derived from the snowline approach $\Delta M_{\mathrm{tsl(meas)}}$ for the three glaciers and for the periods corresponding to the geodetic surveys in m w.e. yr^{-1}.

	$\Delta M_{\mathrm{geod(meas)}}$	$\Delta M_{\mathrm{tsl(meas)}}$
Abramov		
2003-2015	-0.39 ± 0.16	-0.25 ± 0.20
2011-2015	-0.36 ± 0.26	-0.43 ± 0.17
Golubin		
2006–2014	-0.30 ± 0.37	-0.38 ± 0.35
Glacier No. 354		
2003-2012	-0.42 ± 0.07	-0.25 ± 0.31
2012-2015	-0.58 ± 0.31	-0.53 ± 0.43

constrained by snowline observations indicates a significantly less negative mass balance (Fig. 11). For Abramov, a geodetic mass balance of -0.39 ± 0.16 m w.e. yr^{-1} from 27 August 2003 to 1 September 2015 and of -0.36 ± 0.26 m w.e. yr^{-1} from 29 November 2011 to 1 September 2015 was calculated. For the same periods, the snowline model reveals a total mass change of -0.25 ± 0.20 m w.e. yr^{-1} and of -0.43 ± 0.17 m w.e. yr^{-1}, respectively. For the first period, the modelled mass balance con-
5   strained by snowline observations indicates a less negative mass balance, whereas the second period is in good agreement (Table 8 and Fig. 11). For all three glaciers and periods studied the differences are within the error margins.
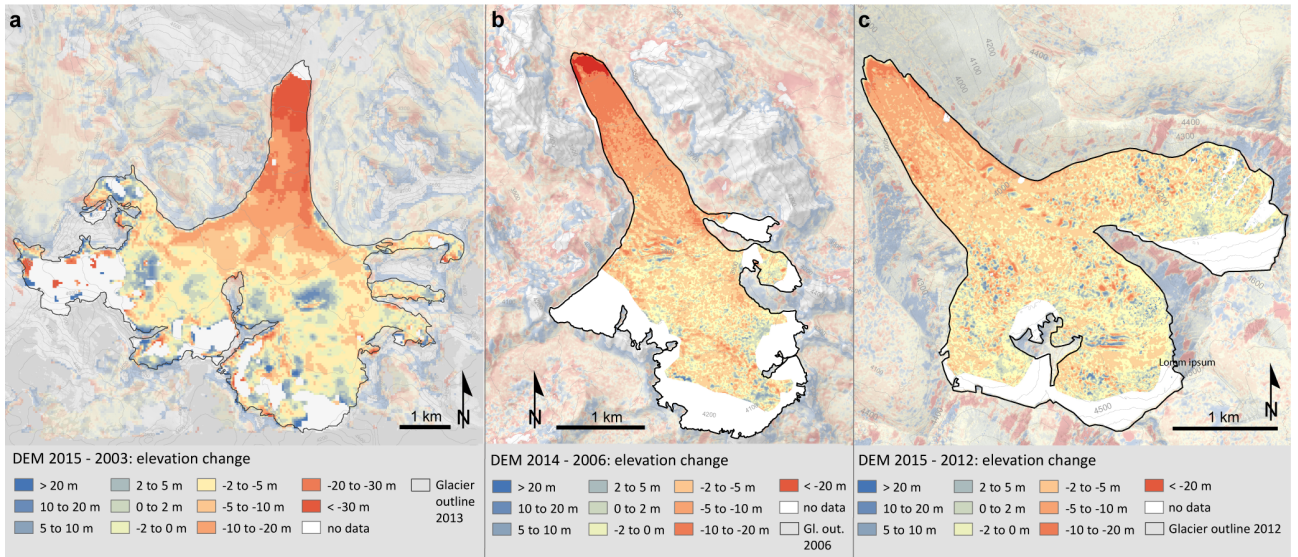
Figure 10. Geodetic mass balance for (**a**) Abramov from 2003 to 2015, (**b**) Golubin from 2006 to 2014 and for (**c**) Glacier No. 354 from 2012 to 2015.
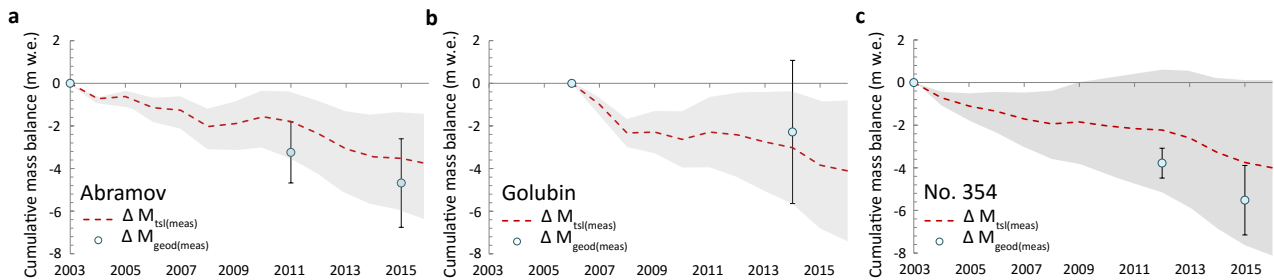
Figure 11. Cumulative snowline-constrained modelled mass change $\Delta M_{\mathrm{tsl(meas)}}$ (red) in comparison to the geodetic mass change $\Delta M_{\mathrm{geod(meas)}}$ (circles) for (**a**) Abramov, (**b**) Golubin and (**c**) Glacier No. 354. The shading indicates the uncertainty range of the mass change from the snowline approach.

6 Discussion

6.1 More accurate modelling through integrating snowline observations

In order to demonstrate the advantage of using snowline observations on repeated remote sensing data throughout the melting season for increasing the confidence in mass balance modelling, we ran the same accumulation and temperature-index model without the use of snowlines or any other direct observations for calibration for all three glaciers from 2004 to 2016 (See Section 3.6). The same constant parameters were used (Table 3). We chose C_{prec} to account for a 20%-measurement error of observed

precipitation (Sevruk, 1981), and a combination for DDF_{ice} (7.0 mm day^{-1} °C^{-1}) and DDF_{snow} (5.5 mm day^{-1} °C^{-1}) as recommended by Hock (2003) for the former Soviet territory, for all three glaciers. Similar values were used to model glaciers in the Tien Shan and Himalayas (e.g. Zhang et al., 2006; Wu et al., 2011; Shea et al., 2015). All parameters were held constant over time. Figure 12 shows the difference between the cumulative SMB derived from our model constrained by snowline observations, and the results obtained with an unconstrained mass balance model. The results clearly indicate the potential of the snowline approach to infer SMB series of unmeasured glaciers without any additional information. The unconstrained mass balance model overestimates mass loss by almost five times for Abramov and for Glacier No. 354, whereas mass loss for Golubin is about three times higher (Fig. 12).
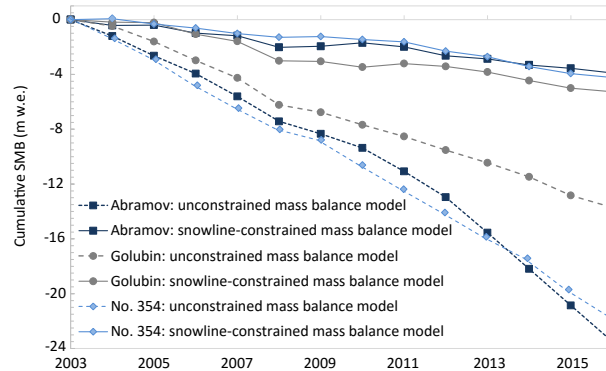
Figure 12. Comparison of the cumulative SMB derived from unconstrained mass balance modelling to the results obtained from snowline-constrained modelling from 2004 to 2016.

6.2 Intercomparison of methods to determine glacier mass balance

A satisfying agreement was found between all three independent methods used to compute glacier-wide mass balance for the three benchmark glaciers in the Central Tien Shan and Pamir-Alay for the past two decades. In the following, we discuss shortcomings and advantages of each method and point out the limitations of the individual approaches.

The snowline model reproduces the direct measurements well and shows a satisfactory performance for all three glaciers (Table 8, 6 and Fig. 13). For Glacier No. 354, a larger misfit between the glaciological SMB and the snowline-constrained model results was found, especially for 2011. A possible reason might be the limited stake network at the initiation of the monitoring programme, errors of the stake readings and an unknown measurement date for some ablation stakes, affecting the calculation of the glaciological SMB for the considered year. Discrepancies between the two approaches are also found for Golubin for 2016 and for Abramov for 2015. For Abramov, summer snowfalls in mid-August 2015 stopped the ablation season early. This pattern is mirrored in the daily SMB derived from the snowline approach. For Golubin, the last snowline observation is from the end of August and matches the field observations. No clear indication of a poor performance of the snowline approach could thus be identified for both glaciers for the considered years.

An important problem is related to the varying measurement periods of the glaciological SMBs for the selected glaciers (Table 2). Due to changing period lengths, the data do not always represent a complete mass-balance year, and might thus not be representative, making comparison of the results with other methods, glaciers and regions difficult. Interpretation of the results, their contextualization and application in other study fields, such as in hydrology or climatology, are also hampered through the varying and irregular investigation periods. Based on our methodology, we are now able to derive homogenous SMBs for comparable periods of the hydrological year.

An important factor limiting the applicability of mass balance modelling constrained by snowline observations is the dependence on good satellite imagery to map the snowline throughout the ablation season. However, the sensitivity analysis (Section 4) shows that a minimum of only two images that are well distributed throughout the ablation season are sufficient to retrieve reliable results. Image availability is most important close to the end of the ablation season. Taking into account the increasing number of satellite sensors that provide a range of possibilities to observe snowlines in the future will partly resolve this limitation. By comparing the snowline-derived daily SMBs for the years in which seasonal in situ measurements are available, we were able to investigate the effect on the results of the two parameters used for model calibration. The mass balance of Golubin is slightly underestimated at the beginning of the ablation season, and hence the modelled melt is also too low (Fig. 13b). This shortcoming of the calibration procedure cannot be overcome without including additional data, such as e.g. measurements of winter snow accumulation which is difficult on remote glaciers.

SMBs inferred from the snowline approach are closely tied to the representativeness of snowline observations. The method might be able to yield reliable SMB estimates for many glaciers in different climatic regimes, for which the transient snowline is an indicator of the surface mass balance. The relationship between the snowline and the SMB can however be importantly challenged when the position of the transient snowline is blurred by fresh snow or superimposed ice. The applicability of the snowline approach presented here can thus be critical when the transient snowline on remote sensing data cannot unambiguously be identified. This is mainly a problem for glaciers with a summer accumulation regime due to frequent fresh snow falls, and glaciers with a high relevance of superimposed ice.
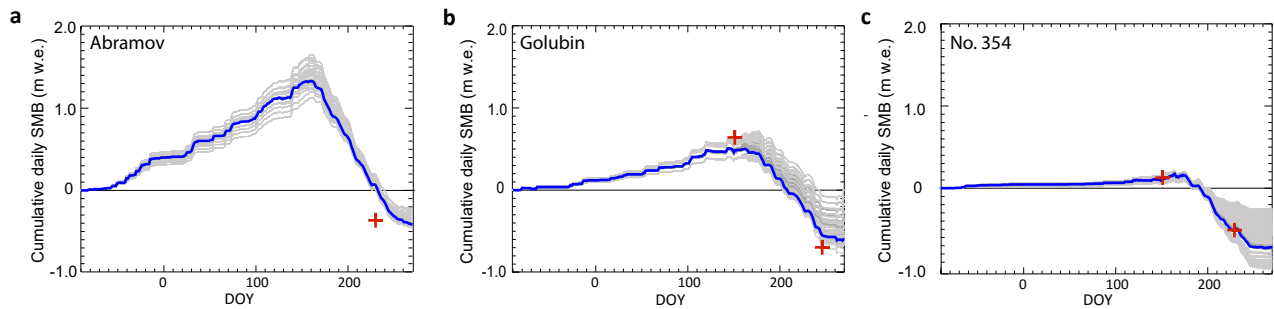
Figure 13. Cumulative daily glacier-wide SMBs inferred from the snowline approach for (**a**) Abramov, (**b**) Golubin and (**c**) Glacier No. 354 for the year 2014 (blue line). The grey lines indicate the spread obtained by using different constant parameters to run the model (Section 4) and the red cross indicates the measured glaciological SMB for both the winter and the annual period.

The geodetic mass balance and the results obtained from the snowline approach agree well, in particular for the recent years (Fig. 11). Overall, a slightly greater mass loss is calculated for Abramov and Glacier No. 354 using DEM differencing. Especially during the earlier part of our study period, the mass balance inferred with the snowline approach seems to be not negative enough. Limitations related to the geodetic approach are mainly connected to the limited stereo acquisitions in the first years of the 21st century. In recent years, image availability strongly increased, but it is still not common to find a suitable scene from the end of the hydrological year for any glacier or region with sufficient quality for a sound geodetic evaluation. Fresh snow or low image contrast (in particular in the accumulation areas) interfere with DEM quality but cannot be avoided and have thus to be corrected for, increasing the uncertainty of the result. We present geodetic mass balances for periods shorter than five years, a critical time interval for an accurate volume-to-mass conversion. Huss (2013) showed a high variability of the volume-to-mass conversion factor for short observation periods ($\leq$ 3 years), especially for glaciers with close-to-zero mass balances in combination with strongly varying mass balance gradients. For the observation periods considered in this study, annual mass balances were predominantly negative but moderate variations of the mass balance gradients have been observed (Barandun et al., 2015; Kronenberg et al., 2016). We identified a rather large elevation change for the short observation periods, and are thus confident that the chosen conversion factor lies within the uncertainty range assigned here (see Section 4).

The glaciological and the modelled results constrained by snowline observations refer to surface mass balance components only. The geodetic mass balance, on the other hand, takes into account the total glacier mass change, thus including internal and basal ablation and accumulation. This is a limiting factor for direct comparison. Evidence of refreezing meltwater in cold firn is reported for all three glaciers (Suslov et al., 1980; Aizen et al., 1997; Dyurgerov and Mikhalenko, 1995) and can have a significant effect on the total mass change. The values used in this study to account for internal and basal mass balance are first-order approximations which improve the comparability between the different methods. However, the uncertainties in these estimates are considerable.

6.3 Comparison to other studies

We performed a comprehensive comparison of long-term averages of mass balance derived from the snowline approach to independent studies based on geodetic surveys using different sensors and modelling, both for the investigated glaciers as well as for the regional mass budget (Fig. 14). Note that the study periods vary between the different studies and results might thus not be directly comparable.

For Abramov, we find mass balances inbetween the results derived by Gardelle et al. (2013) and Brun et al. (2017) based on the comparison of DEMs, overlapping within the respective uncertainty ranges. Mass changes reported by Gardelle et al. (2013) are most likely too positive as SRTM C-Band penetration depth into snow (Kääb et al., 2015; Berthier et al., 2016) might have been underestimated for the cold and dry snow of accumulation areas (Dehecq et al., 2016). The average mass balance for Abramov of -0.38 ± 0.10 m w.e. yr^{-1} (2002-2014) derived by Brun et al. (2017) using multi-temporal optical ASTER DEMs indicates a stronger mass loss than the results obtained with the snowline approach. We note, however, that the start and end dates of their geodetic mass balance assessment represent a mean over a mosaic of different dates, thus hampering direct

comparison. In addition, the differences are still within their error bounds. The results by Brun et al. (2017) are in line with the geodetic mass balance calculated in the present study for the period 2003 to 2015 based on high-resolution satellite images.

For Golubin, the inferred mass balance is in close agreement with the geodetic mass change reported by Bolch (2015) (Fig. 14b). Brun et al. (2017) computed a mass balance of -0.04 ± 0.19 m w.e. yr^{-1} for $\approx$2002-2013, which is consistently less negative than our estimate but still lies within the respective error bounds. For Glacier No. 354, an excellent agreement between all available mass balance assessments was found (Fig. 14c). Brun et al. (2017) reported a mass balance of -0.46 ± 0.19 m w.e. yr^{-1} for $\approx$2002-2014.

We also compared our results for the investigated glaciers to region-wide assessments in order to investigate their regional representativeness (Fig. 14d-f). Brun et al. (2017) divided the Pamir-Alay and the Pamir into two different regions, whereas Gardner et al. (2013), Gardelle et al. (2013), Kääb et al. (2015) and Farinotti et al. (2015) did not make this distinction. For the Pamir, widely varying mass balance estimates were presented by the different studies, which might be related to important methodological differences and inconsistent time periods considered. Our results for Abramov are close to the average of the regional studies (Fig. 14d). The interannual variability and, in particular, a very negative mass balance in 2008 and a positive balance in 2010 for Abramov found in the present study agrees well with modelled mass balance series reported by Pohl et al. (2017) for the Pamir from 2002 to 2013. The snowline-constrained modelled mass balance for Golubin agrees with the region-wide estimates by Brun et al. (2017) but indicates smaller mass losses than other large-scale studies (Fig. 14e). Close agreement between the different regional studies is found for the Central/Inner Tien Shan, where Glacier No. 354 is located (Fig. 14f).

7 Conclusions

In this study we used three independent methods to reconstruct robust mass balance series at high temporal resolution for Abramov, Golubin and Glacier No. 354 located in the Pamir-Alay and Tien Shan mountains for the past two decades – a period for which only little is known about glacier behaviour. We proposed a methodology to derive glacier SMB series for unmeasured glaciers based on mass balance modelling constrained by repeated snowline observations relying either on in situ temperature and precipitation data or climate Reanalysis datasets. We recommend including snowline observations in the glacier monitoring strategy to reduce uncertainty and to increase robustness of the data. We used extensive geodetic and glaciological surveys to validate the results and found satisfying agreement between the independent methods. Our snowline approach reproduced observed annual to decadal SMB for all three glaciers and enabled the calculation of daily SMBs for arbitrary periods, and is, hence, capable of covering the entire hydrological year based on minimal data input. Some of the shortcomings of the glaciological and geodetic surveys could thus be overcome.

The results of all three methods confirm a continuous mass loss of the three glaciers Abramov, Golubin and Glacier No. 354 since $\approx$2000 but no clear SMB trend could be identified for the time period considered. Our results suggest a slightly less negative SMBs for Abramov of -0.30 ± 0.19 m w.e. yr^{-1} located in the Pamir-Alay than for the Tien Shan glaciers Golubin of -0.41 ± 0.33 m w.e. yr^{-1} and Glacier No. 354 of -0.36 ± 0.32 m w.e. yr^{-1} from 2004 to 2016. Periods of almost balanced mass
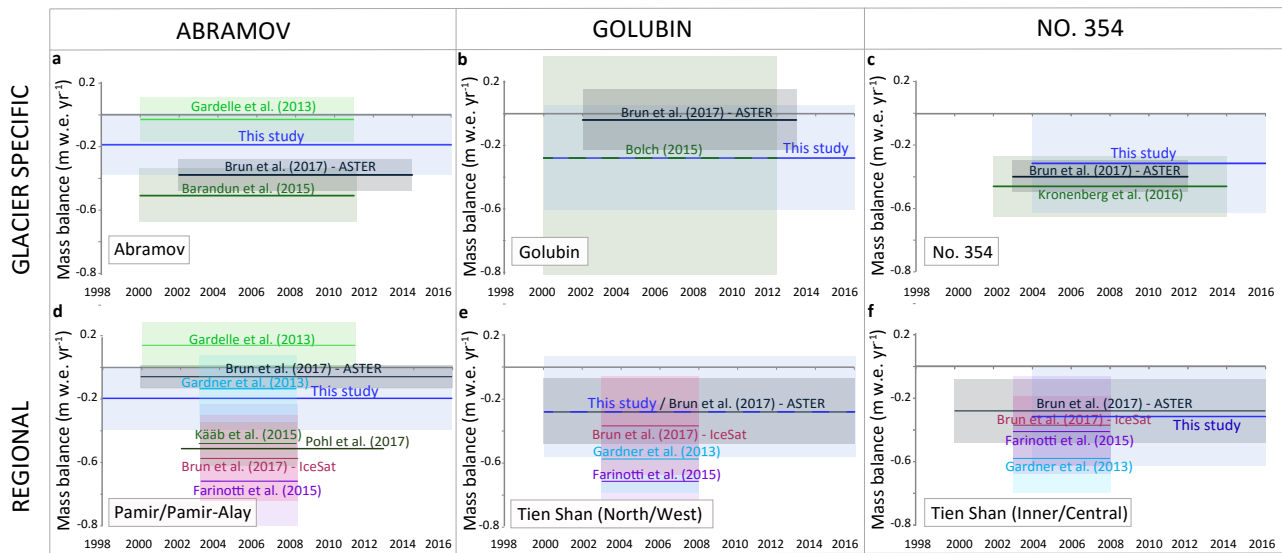
Figure 14. Long-term average mass balances from various studies in comparison with the snowline-constrained modelled mass balance for (**a**) Abramov, (**b**) Golubin, (**c**) Glacier No. 354. Results from the snowline approach for the three glaciers are compared to region-wide mass balance estimates for (**d**) the Pamir, for (**e**) Tien Shan (North/West) and for (**f**) the Tien Shan (Inner/Central). Lines indicate the mean annual mass balance over the respective periods for each study, and shaded squares represent the corresponding uncertainty. For the study by Brun et al. (2017) results based on ASTER DEMs and IceSat are presented separately.

budgets were observed from 2002 to 2005 and from 2009 to 2011. The mass balance of 2006 to 2008 was very negative for Abramov and Golubin. Glacier No. 354 showed a weaker interannual variability than the other two glaciers. Model sensitivity experiments revealed a relatively small sensitivity to the input parameters and the meteorological data used, indicating a considerable advantage in comparison to conventional mass balance modelling that does not include direct glacier-specific

5   observations. Our results show that with a minimum of two snowline observations, ideally at the beginning and the end of the ablation season, reliable estimates of the annual SMB can be inferred.

At present, mass balance observations in the Pamir and Tien Shan are relatively sparse but crucially needed to improve understanding of glacier behaviour in the region and its effect on future water availability. Direct measurements are important but costly and laborious and require an immense logistic effort. For remote and unmonitored regions and countries, lacking

10   in financial resources and infrastructure to support such monitoring programmes, our proposed approach delivers a tool for investigating and reconstructing the SMBs of unmeasured and remote glaciers with minimal effort. The integration of snowline observations into conventional modelling is shown to be highly beneficial for filling the gaps in long-term SMB series for periods for which direct glaciological measurements were discontinued or are missing completely.

Acknowledgements. This study is supported by the Swiss National Science Foundation (SNSF), grant 200021_155903. Additional support by the German Federal Foreign Office in the frame of the CAWa project (http://www.cawa-project.net) and the support of the Federal Office of Meteorology and Climatology MeteoSwiss through the project Capacity Building and Twinning for Climate Observing Systems (CATCOS) Phase 1 & 2, Contract nos. $7F$-08114.1, $7F$-08114.02.01, between the Swiss Agency for Development and Cooperation (SDC)

5   and MeteoSwiss as well as the project CICADA (Cryospheric Climate Services for improved Adaptation), and contract no. 81049674 between Swiss Agency for Development and Cooperation and the University of Fribourg is equally acknowledged. E. Berthier acknowledges support from the French Space Agency (CNES) and the Programme National de Télédétection Spatiale grant PNTS$-2016-01$. A. Kääb and T. Bolch acknowledges funding by ESA (Glaciers_cci project 4000109873/14/I-NB), and the European Union Seventh Framework Program (FP7) under European Research Council (ERC) contract 320816. We thank F. Brun for providing the elevation change data of Abramov, Golubin

10   and Glacier No. 354. J. Corripio is acknowledged for the software to georeference oblique photographs. We extend our thanks as well to T. Saks, A. Ghirlanda, A. Gafurov, M. Kronenberg, D. Sciboz and all others who contributed with fieldwork. We are also grateful for the collaboration of Central Asian Institute for Applied Geosciences, especially to B. Moldobekov for his continuous support. The Kumtor Gold Company provided the meteorological data. We thank S. Braun-Clarke for the proofreading and linguistic revision. Constructive comments by the anonymous reviewer and Prof. Dr. M. Pelto were very helpful to finalize the manuscript.

References

Aizen, V.: Reconstruktiya balansa massy lednika Golubina [Golubin glacier mass balance reconstruction], Mater. Glyatsiol. Issled, 62, 119–126, 1988.

Aizen, V. B., Aizen, E. M., and Melack, J. M.: Climate, snow cover, glaciers, and runoff in the Tien Shan, central Asia, JAWRA Journal of the American Water Resources Association, 31, 1113–1129, 1995.

Aizen, V. B., Aizen, E. M., Melack, J. M., and Dozier, J.: Climatic and hydrologic changes in the Tien Shan, central Asia, Journal of Climate, 10, 1393–1404, doi:10.1175/1520-0442(1997)010<1393:CAHCIT>2.0.CO;2, 1997.

Aizen, V. B., Kuzmichenok, V. A., Surazakov, A. B., and Aizen, E. M.: Glacier changes in the Tien Shan as determined from topographic and remotely sensed data, Global and Planetary Change, 56, 328–340, 2007.

Alpert, P.: Mesoscale indexing of the distribution of orographic precipitation over high mountains, Journal of climate and applied meteorology, 25, 532–545, 1986.

Barandun, M., Huss, M., Sold, L., Farinotti, D., Azisov, E., Salzmann, N., Usubaliev, R., Merkushkin, A., and Hoelzle, M.: Re-analysis of seasonal mass balance at Abramov glacier 1968–2014, Journal of Glaciology, 61, 1103–1117, doi:10.3189/2015JoG14J239, 2015.

Berthier, E., Vincent, C., Magnússon, E., Gunnlaugsson, Á., Pitte, P., Le Meur, E., Masiokas, M., Ruiz, L., Pálsson, F., Belart, J., et al.: Glacier topography and elevation changes derived from Pléiades sub-meter stereo images, The Cryosphere, 8, 2275–2291, doi:10.5194/tc-8-2275-2014, 2014.

Berthier, E., Cabot, V., Vincent, C., and Six, D.: Decadal Region-Wide and Glacier-Wide Mass Balances Derived from Multi-Temporal ASTER Satellite Digital Elevation Models. Validation over the Mont-Blanc Area, Frontiers in Earth Science, 4, 63, 2016.

Bolch, T.: Glacier area and mass changes since 1964 in the Ala Archa Valley, Kyrgyz Ala-Too, northern Tien Shan, Ice and Snow, pp. 28–39, doi:10.15356/2076-6734-2015-1-28-39, 2015.

Braithwaite, R. J.: Short Notes: Can the Mass Balance of a Glacier be Estimated from its Equilibrium-Line Altitude?, Journal of Glaciology, 30, 364–368, 1984.

Braithwaite, R. J.: Positive degree-day factors for ablation on the Greenland ice sheet studied by energy-balance modelling, Journal of Glaciology, 41, 153–160, doi:10.3189/S0022143000017846, 1995.

Brun, F., Berthier, E., Wagnon, P., Kääb, A., and Treichler, D.: A spatially resolved estimate of High Mountain Asia glacier mass balances, 2000-2016., Nature Geoscience, 10, 668, doi:10.1038/ngeo2999, 2017.

Chen, Y., Li, W., Deng, H., Fang, G., and Li, Z.: Changes in Central Asia's Water Tower: Past, Present and Future, Scientific reports, 6, 35 458, doi:10.1038/srep35458, 2016.

Chinn, T.: Glacier fluctuations in the Southern Alps of New Zealand determined from snowline elevations, Arctic and alpine research, pp. 187–198, doi:10.2307/1551901, 1995.

Chinn, T.: New Zealand glacier response to climate change of the past 2 decades, Global and Planetary Change, 22, 155–168, doi:10.1016/S0921-8181(99)00033-8, 1999.

Cogley, J., Hock, R., Rasmussen, L., Arendt, A., Bauder, A., Braithwaite, R., Jansson, P., Kaser, G., Möller, M., Nicholson, L., and Zemp, M.: Glossary of glacier mass balance and related terms, IHP-VII technical documents in hydrology No. 86, IACS Contribution No. 2, doi:10.1657/1938-4246-44.2.256b, 2011.

Corripio, J.: Snow surface albedo estimation using terrestrial photography, International Journal of Remote Sensing, 25, 5705–5729, doi:10.1080/01431160410001709002, 2004.

Dee, D., Uppala, S., Simmons, A., Berrisford, P., Poli, P., Kobayashi, S., Andrae, U., Balmaseda, M., Balsamo, G., Bauer, P., Bechtold, P., Beljaars, A. C. M., van de Berg, L., Bidlot, J., Bormann, N., Delsol, C., Dragani, R., Fuentes, M., Geer, A. J., Haimberger, L., Healy, S., Hersbach, H., Hólm, E., Isaksen, L., Kållberg, P., Köhler, M., Matricardi, M., McNally, P., Monge-Sanz, B., Morcrette, J., Park, B., Peubey, C., de Rosnay, P., Tavolato, C., Thépaut, J., and Vitart, F.: The ERA-Interim reanalysis: configuration and performance of the data assimilation system, Quarterly Journal of the Royal Meteorological Society, 137, 553–597, doi:10.1002/qj.828, 2011.

Dehecq, A., Millan, R., Berthier, E., Gourmelen, N., Trouvé, E., and Vionnet, V.: Elevation changes inferred from TanDEM-X data over the Mont-Blanc area: Impact of the X-band interferometric bias, IEEE Journal of Selected Topics in Applied Earth Observations and Remote Sensing, 9, 3870–3882, doi:10.1109/JSTARS.2016.2581482, 2016.

Duethmann, D., Peters, J., Blume, T., Vorogushyn, S., and Güntner, A.: The value of satellite-derived snow cover images for calibrating a hydrological model in snow-dominated catchments in Central Asia, Water Resources Research, 50, 2002–2021, doi:10.1002/2013WR014382, 2014.

Dyurgerov, M.: Substitution of long-term mass balance data by measurements of one summer, Zeitschrift für Gletscherkunde und Glazialgeologie, 32, 177–184, 1996.

Dyurgerov, M. and Mikhalenko, V.: Oledeneniye Tien Shanya [Glaciation of Tien Shan], VINITI, Moscow [in Russian], 1995.

Dyurgerov, M., Mikhalenko, V., Kunakhovitch, M., Ushnurtsev, S., Liu, C., and Xie, Z.: On the cause of glacier mass balance variations in the Tian Shan mountains, GeoJournal, 33, 311–317, doi:10.1007/BF00812879, 1994.

Farinotti, D., Longuevergne, L., Moholdt, G., Duethmann, D., Mölg, T., Bolch, T., Vorogushyn, S., and Güntner, A.: Substantial glacier mass loss in the Tien Shan over the past 50 years, Nature Geoscience, 8, 716–722, doi:10.1038/ngeo2513, 2015.

Fujita, K., Takeuchi, N., Nikitin, S., Surazakov, A., Okamoto, S., Aizen, V., and Kubota, J.: Favorable climatic regime for maintaining the present-day geometry of the Gregoriev Glacier, Inner Tien Shan, The Cryosphere, 5, 539, doi:10.5194/tc-5-539-2011, 2011.

Gao, X., Ye, B., Zhang, S., Qiao, C., and Zhang, X.: Glacier runoff variation and its influence on river runoff during 1961–2006 in the Tarim River Basin, China, Science China Earth Sciences, 53, 880–891, doi:10.1007/s11430-010-0073-4, 2010.

Gardelle, J., Berthier, E., Arnaud, Y., and Kääb, A.: Region-wide glacier mass balances over the Pamir-Karakoram-Himalaya during 1999–2011, The Cryosphere, 7, 1263–1286, doi:10.5194/tc-7-1263-2013, 2013.

Gardner, A., Moholdt, G., Cogley, J., Wouters, B., Arendt, A., Wahr, J., Berthier, E., Hock, R., Pfeffer, W., Kaser, G., Ligtenberg, S., Bolch, T., Sharp, M., Hagen, J., van den Broeke, M., and Paul, F.: A Reconciled Estimate of Glacier Contributions to Sea Level Rise: 2003 to 2009, Science, 340, 852–857, doi:10.1126/science.1234532, 2013.

GCOS: The Global Observing System for Climate: Implementation Needs, GCOS, 325p, 180, 2016.

Glazirin, G., Kamnyanskii, G., and Perziger, F.: Regime of the Abramov glacier, Leningrad: Hydrometeo Publishing, 1993.

Goerlich, F., Bolch, T., Mukherjee, K., and Pieczonka, T.: Glacier Mass Loss during the 1960s and 1970s in the Ak-Shirak Range (Kyrgyzstan) from Multiple Stereoscopic Corona and Hexagon Imagery, Remote Sensing, 9, 275, doi:10.3390/rs9030275, 2017.

Hock, R.: A distributed temperature-index ice-and snowmelt model including potential direct solar radiation, Journal of Glaciology, 45, 101–111, doi:10.1017/S0022143000003087, 1999.

Hock, R.: Temperature index melt modelling in mountain areas, Journal of Hydrology, 282, 104–115, doi:10.1016/S0022-1694(03)00257-9, 2003.

Hock, R., Kootstra, D.-S., and Reijmer, C.: Deriving glacier mass balance from accumulation area ratio on Storglaciären, Sweden, IAHS-AISH publication, pp. 163–170, 2007.

Hoelzle, M., Azisov, E., Barandun, M., Huss, M., Farinotti, D., Gafurov, A., Hagg, W., Kenzhebaev, R., Kronenberg, M., Machguth, H., et al.: Re-establishing glacier monitoring in Kyrgyzstan and Uzbekistan, Central Asia, Geoscientific Instrumentation, Methods and Data Systems, 6, 397, doi:10.5194/gi-6-397-2017, 2017.

Hulth, J., Rolstad Denby, C., and Hock, R.: Estimating glacier snow accumulation from backward calculation of melt and snowline tracking, Annals of Glaciology, 64, 1–7, doi:10.3189/2013AoG62A083, 2013.

Huss, M.: Density assumptions for converting geodetic glacier volume change to mass change, The Cryosphere, 7, 877–887, doi:10.5194/tc-7-877-2013, 2013.

Huss, M. and Hock, R.: Global-scale hydrological response to future glacier mass loss, Nature Climate Change, p. 1, doi:10.1038/s41558-017-0049-x, 2018.

Huss, M., Bauder, A., Funk, M., and Hock, R.: Determination of the seasonal mass balance of four Alpine glaciers since 1865, Journal of Geophysical Research: Earth Surface, 113, doi:10.1029/2007JF000803, 2008.

Huss, M., Bauder, A., and Funk, M.: Homogenization of long-term mass balance time series, Annals of Glaciology, 50, 198–206, doi:10.3189/172756409787769627, 2009.

Huss, M., Sold, L., Hoelzle, M., Stokvis, M., Salzmann, N., Farinotti, D., and Zemp, M.: Towards remote monitoring of sub-seasonal glacier mass balance, Annals of Glaciology, 53, 278–286, doi:10.3189/2012JoG11J216, 2013.

Kääb, A., Treichler, D., Nuth, C., and Berthier, E.: Brief Communication: Contending estimates of 2003–2008 glacier mass balance over the Pamir–Karakoram–Himalaya, The Cryosphere, 9, 557–564, doi:10.5194/tc-9-557-2015, 2015.

Kamniansky, G. and Pertziger, F.: Optimization of mountain glacier mass balance measurements, Zeitschrift für Gletscherkunde und Glazialgeologie, 32, 167–75, 1996.

Kaser, G., Großhauser, M., and Marzeion, B.: Contribution potential of glaciers to water availability in different climate regimes, Proceedings of the National Academy of Sciences, 107, 20 223–20 227, doi:10.1073/pnas.1008162107, 2010.

Kenzhebaev, R., Barandun, M., Kronenberg, M., Chen, Y., Usubaliev, R., and Hoelzle, M.: Mass balance observations and reconstruction for Batysh Sook Glacier, Tien Shan, from 2004 to 2016, Cold Regions Science and Technology, 135, 76–89, 2017.

Korona, J., Berthier, E., Bernard, M., Rémy, F., and Thouvenot, E.: SPIRIT. SPOT 5 stereoscopic survey of polar ice: reference images and topographies during the fourth International Polar Year (2007–2009), ISPRS Journal of Photogrammetry and Remote Sensing, 64, 204–212, doi:10.1016/j.isprsjprs.2008.10.005, 2009.

Kronenberg, M., Barandun, M., Hoelzle, M., Huss, M., Farinotti, D., Azisov, E., Usubaliev, R., Gafurov, A., Petrakov, D., and Kääb, A.: Mass-balance reconstruction for Glacier No. 354, Tien Shan, from 2003 to 2014, Annals of Glaciology, 57, 92–102, doi:10.3189/2016AoG71A032, 2016.

Kulkarni, A. V.: Mass balance of Himalayan glaciers using AAR and ELA methods, Journal of Glaciology, 38, 101–104, doi:10.3189/S0022143000009631, 1992.

Kulkarni, A. V.: Monitoring Himalayan cryosphere using remote sensing techniques, Journal of the Indian Institute of Science, 90, 457–469, 2012.

Kulkarni, A. V., Rathore, B., and Alex, S.: Monitoring of glacial mass balance in the Baspa basin using accumulation area ratio method, Current Science, pp. 185–190, 2004.

Kulkarni, A. V., Rathore, B., Singh, S., and Bahuguna, I.: Understanding changes in the Himalayan cryosphere using remote sensing techniques, International Journal of Remote Sensing, 32, 601–615, doi:10.1080/01431161.2010.517802, 2011.

LaChapelle, E.: Assessing glacier mass budgets by reconnaissance aerial photography, Journal of Glaciology, 4, 290–297, 1962.

Liu, Q. and Liu, S.: Response of glacier mass balance to climate change in the Tianshan Mountains during the second half of the twentieth century, Climate dynamics, 46, 303–316, doi:10.1007/s00382-015-2585-2, 2016.

Lliboutry, L.: Traité de glaciologie: Glaciers, Variations du climat, Sols gelés, vol. 2, Masson, 1965.

Marti, R., Gascoin, S., Berthier, E., De Pinel, M., Houet, T., and Laffly, D.: Mapping snow depth in open alpine terrain from stereo satellite imagery, The Cryosphere, 10, 1361, doi:10.5194/tc-10-1361-2016, 2016.

Mernild, S. H., Pelto, M., Malmros, J. K., Yde, J. C., Knudsen, N. T., and Hanna, E.: Identification of snow ablation rate, ELA, AAR and net mass balance using transient snowline variations on two Arctic glaciers, Journal of Glaciology, 59, 649–659, doi:10.3189/2013JoG12J221, 2013.

Munia, H., Guillaume, J., Mirumachi, N., Porkka, M., Wada, Y., and Kummu, M.: Water stress in global transboundary river basins: significance of upstream water use on downstream stress, Environmental Research Letters, 11, 014 002, doi:10.5194/tc-10-1361-2016, 2016.

Nuth, C. and Kääb, A.: Co-registration and bias corrections of satellite elevation data sets for quantifying glacier thickness change, The Cryosphere, 5, 271–290, doi:10.5194/tc-5-271-2011, 2011.

Østrem, G.: The transient snowline and glacier mass balance in southern British Columbia and Alberta, Canada, Geografiska Annaler. Series A. Physical Geography, pp. 93–106, 1973.

Østrem, G.: ERTS data in glaciology—an effort to monitor glacier mass balance from satellite imagery, Journal of Glaciology, 15, 403–415, 1975.

Paul, F., Barrand, N., Baumann, S., Berthier, E., Bolch, T., Casey, K., Frey, H., Joshi, S., Konovalov, V., Le Bris, R., et al.: On the accuracy of glacier outlines derived from remote-sensing data, Annals of Glaciology, 54, 171–182, doi:10.3189/2013AoG63A296, 2013.

Paul, F., Bolch, T., Kääb, A., Nagler, T., Nuth, C., Scharrer, K., Shepherd, A., Strozzi, T., Ticconi, F., Bhambri, R., et al.: The glaciers climate change initiative: Methods for creating glacier area, elevation change and velocity products, Remote Sensing of Environment, 162, 408–426, doi:10.1016/j.rse.2013.07.043, 2015.

Pelto, M.: Satellite identification of transient snowline variation during the melt season for mass balance assessment Taku and Brady Glacier, Alaska, in: 67th Eastern Snow Conference Jiminy Peak Mountain Resort, Hancock, MA, USA, pp. 51–60, 2010.

Pelto, M., Kavanaugh, J., and McNeil, C.: Juneau Icefield mass balance program 1946–2011, Earth System Science Data, 5, 319–330, doi:10.5194/essd-5-319-2013, 2013.

Pertziger, F.: Abramov Glacier data reference book: climate, runoff, mass balance, Central Asian Regional Research Hydrometeorological Institute named by VA Bugaev, Tashkent, Republic of Uzbekistan, 279p, 1996.

Pieczonka, T. and Bolch, T.: Region-wide glacier mass budgets and area changes for the Central Tien Shan between˜ 1975 and 1999 using Hexagon KH-9 imagery, Global and Planetary Change, 128, 1–13, doi:10.1016/j.gloplacha.2014.11.014, 2015.

Pieczonka, T., Bolch, T., Junfeng, W., and Shiyin, L.: Heterogeneous mass loss of glaciers in the Aksu-Tarim Catchment (Central Tien Shan) revealed by 1976 KH-9 Hexagon and 2009 SPOT-5 stereo imagery, Remote Sensing of Environment, 130, 233–244, doi:10.1016/j.rse.2012.11.020, 2013.

Pohl, E., Gloaguen, R., Andermann, C., and Knoche, M.: Glacier melt buffers river runoff in the Pamir Mountains, Water Resources Research, 53, 2467–2489, doi:10.1002/2016WR019431, 2017.

Rabatel, A., Dedieu, J.-P., and Vincent, C.: Using remote-sensing data to determine equilibrium-line altitude and mass-balance time series: validation on three French glaciers, 1994–2002, Journal of Glaciology, 51, 539–546, doi:10.3189/172756505781829106, 2005.

Rabatel, A., Dedieu, J.-P., Thibert, E., Letreguilly, A., and Vincent, C.: 25 years (1981–2005) of equilibrium-line altitude and mass-balance reconstruction on Glacier Blanc, French Alps, using remote-sensing methods and meteorological data, Journal of Glaciology, 54, 307–314, doi:10.3189/002214308784886063, 2008.

Rabatel, A., Bermejo, A., Loarte, E., Soruco, A., Gomez, J., Leonardini, G., Vincent, C., and Sicart, J. E.: Can the snowline be used as an indicator of the equilibrium line and mass balance for glaciers in the outer tropics?, Journal of Glaciology, 58, 1027–1036, doi:10.3189/2012JoG12J027, 2012.

Rabatel, A., Letréguilly, A., Dedieu, J., and Eckert, N.: Changes in glacier equilibrium-line altitude in the western Alps from 1984 to 2010: evaluation by remote sensing and modeling of the morpho-topographic and climate controls, The Cryosphere, 7, p–1455, doi:10.5194/tc-7-1455-2013, 2013.

Rabatel, A., Dedieu, J. P., and Vincent, C.: Spatio-temporal changes in glacier-wide mass balance quantified by optical remote sensing on 30 glaciers in the French Alps for the period 1983–2014, Journal of Glaciology, 62, 1153–1166, doi:10.1017/jog.2016.113, 2016.

Rabatel, A., Sirguey, P., Drolon, V., Maisongrande, P., Arnaud, Y., Berthier, E., Davaze, L., Dedieu, J.-P., and Dumont, M.: Annual and Seasonal Glacier-Wide Surface Mass Balance Quantified from Changes in Glacier Surface State: A Review on Existing Methods Using Optical Satellite Imagery, Remote Sensing, 9, 507, doi:10.3390/rs9050507, 2017.

Schaner, N., Voisin, N., Nijssen, B., and Lettenmaier, D. P.: The contribution of glacier melt to streamflow, Environmental Research Letters, 7, 034 029, doi:10.1088/1748-9326/7/3/034029, 2012.

Sevruk, B.: Methodische Untersuchungen des systematischen Messfehlers der Hellmann-Regenmesser im Sommerhalbjahr in der Schweiz.(Methodical investigations of the systematic error of the Hellmann raingauge in the summer season in the Switzerland). Versuchsanstalt für Wasserbau, Hydrologie und Glaziologie, ETH Zürich, Mitt. 52, 296 S, Ph.D. thesis, ETH Zurich, 1981.

Shea, J., Immerzeel, W., Wagnon, P., Vincent, C., and Bajracharya, S.: Modelling glacier change in the Everest region, Nepal Himalaya, The Cryosphere, 9, 1105–1128, doi:10.5194/tc-9-1105-2015, 2015.

Shean, D. E., Alexandrov, O., Moratto, Z. M., Smith, B. E., Joughin, I. R., Porter, C., and Morin, P.: An automated, open-source pipeline for mass production of digital elevation models (DEMs) from very-high-resolution commercial stereo satellite imagery, ISPRS Journal of Photogrammetry and Remote Sensing, 116, 101–117, doi:10.1016/j.isprsjprs.2016.03.012, 2016.

Sorg, A., Bolch, T., Stoffel, M., Solomina, O., and Beniston, M.: Climate change impacts on glaciers and runoff in Tien Shan (Central Asia), Nature Climate Change, 2, 725–731, doi:10.1038/nclimate1592, 2012.

Stocker, T. F., Qin, D., Plattner, G.-K., Tignor, M., Allen, S. K., Boschung, J., Nauels, A., Xia, Y., Bex, B., and Midgley, B.: IPCC, 2013: climate change 2013: the physical science basis. Contribution of working group I to the fifth assessment report of the intergovernmental panel on climate change, 2013.

Suslov, B., Akbarov, A., and Yemelyanov, J.: Abramov glacier, Hydrometeoizdat, Leningrad, 1980.

Unger-Shayesteh, K., Vorogushyn, S., Farinotti, D., Gafurov, A., Duethmann, D., Mandychev, A., and Merz, B.: What do we know about past changes in the water cycle of Central Asian headwaters? A review, Global and Planetary Change, 110, 4–25, doi:10.1016/j.gloplacha.2013.02.004, 2013.

Varis, O.: Curb vast water use in central Asia, Nature, 514, 27–30, doi:10.1038/514027a, 2014.

Wang, Q., Yi, S., Chang, L., and Sun, W.: Large-scale seasonal changes in glacier thickness across High Mountain Asia, Geophysical Research Letters, doi:10.1002/2017GL075300, 2017.

WGMS: Glacier mass balance bulletin no. 12, vol. 12 of *Glacier Mass Balance Bulletin*, ICSU (WDS) / IUGG(IACS) / UNEP / UNESCO / WMO, World Glacier Monitoring Service, Zürich, doi:10.5904/wgms-fog-2013-11, 2013.

Wu, L., Li, H., and Wang, L.: Application of a degree-day model for determination of mass balance of Urumqi Glacier No. 1, eastern Tianshan, China, Journal of Earth Science, 22, 470–481, doi:10.1007/s12583-011-0201-x, 2011.

Wu, Y., He, J., Guo, Z., and Chen, A.: Limitations in identifying the equilibrium-line altitude from the optical remote-sensing derived snowline in the Tien Shan, China, Journal of Glaciology, 60, 1093, doi:10.3189/2014JoG13J221, 2014.

5 Young, G.: The mass balance of Peyto glacier, Alberta, Canada, 1965 to 1978, Arctic and Alpine Research, pp. 307–318, 1981.

Zhang, Y., Liu, S., Xie, C., and Ding, Y.: Application of a degree-day model for the determination of contributions to glacier meltwater and runoff near Keqicar Baqi glacier, southwestern Tien Shan, Annals of Glaciology, 43, 280–284, doi:10.3189/172756406781812320, 2006.